Polarforschung 88 (2), 99 – 123, 2018 (erschienen 2019)

Glacial-geodetic long-term study on mass balance and ice dynamics near the equilibrium line of the Greenland ice sheet.

by Manfred Stober[1], Jörg Hepperle[1]

Abstract: The recent acceleration of mass loss of the Greenland ice sheet, as determined from large-scale, satellite-derived geodetic and gravimetric observations, is well documented. However, long-term *in situ* elevation change measurements are scarce. Here, we present a 23-year time series (1991 to 2014) of bi-annual *in situ* geodetic observations at two sites in West Greenland. Repeated GPS measurements at Swiss Camp (1170 m a.s.l.) and 15 km downglacier at site ST2 (1000 m a.s.l.) were used to determine elevation changes, ice flow velocities, and strain rates. Meteorological observations were used to interpret the results. These were compared to satellite-derived evaluations. Surface elevation at Swiss Camp dropped by 14.4 m between 1991 and 2014 (0.62 m/year on average) with accelerated elevation drops in recent years. The same tendency was also apparent at ST2. Here the surface elevation dropped by 12.2 m between 2004 and 2014 (1.2 m/year on average). The elevation changes were not constant over the survey areas, there were, however, pronounced systematic local differences. The causes of these (e.g. albedo, humidity, etc.) have not yet been established. The velocity of flow does not behave uniformly. At SWC, the ice flows faster (0.32 m/d) than at ST2 (0.19 m/d), and although at SWC acceleration arises, ST2 demonstrates a reduction in speed, probably because of the ascending border mountains. Strain rates vary strongly and show that the local underground of the moved measuring field affects the results strongly. The strain rates in longitudinal direction between both sites are negative, indicating compression of the ice, which results in dynamic thickening. The influence of individual meteorological parameters on the elevation changes was examined using correlation analysis. However, significant correlations were rarely found; in both survey areas these were most clear for the summer albedo. Air temperature and net radiation proved to be less relevant. Comparisons of the geodetic mass balance with the specific SMB from stake measurements show different results. At SWC, the cumulative geodetic mass balance from 1991 to 2014 results in -13.0 m w.e, and SMB from stakes -10.1 m w.e (2014). The dynamic portion results from the difference in relation to the geodetically-determined mass balance. The results at SWC and at ST2 are contradictory. The dynamic part is derived from the strain rates using the continuity (incompressibility) condition. However, consistent results appear only at the beginning of our measurements. Remote sensing results were compared to ground truths with GPS. ICESat altimetry from 2005 demonstrates surface height deviations of -0.13 ± 0.06 m on average. Elevation changes from CryoSat-2 between 2011 and 2014 differ by 0.24 m/a (SWC) and 0.48 m/a (ST2). Heights from a TanDEM-X elevation model in August 2014 show an offset from the GPS elevation model of 3.14 ±0.025 m, the standard deviation of one point being 1.07 m. The ice flow velocity from Sentinel-1 IW, TerraSAR-X, and ALOS PALSAR was compared to ground measurements with GPS. Data from the years 2010–2017 mostly agree well (with the exception of PALSAR) within the measuring accuracy of the satellite procedures.

Zusammenfassung: Das Studium der Eismassenänderung von Grönland ist ein zentraler Forschungsbereich zum Einfluss des Klimawandels. Neben mehreren Methoden zur Bestimmung der Eismassenbilanz (Surface Mass Balance / SMB, Satelliten-Gravimetrie, Satelliten-Altimetrie) können auch geodätische Messungen auf der Eisoberfläche angewandt werden. Diese sind selten, weil sehr aufwändig durchzuführen. Mit dem Forschungsprojekt der HFT Stuttgart werden mittels terrestrischer geodätischer Messungen (GNSS/GPS) in zwei begrenzten Messgebieten folgende Aspekte untersucht: Höhenänderung der Eisoberfläche an konkreten Punkten sowie über eine Fläche (Bestimmung digitaler Höhenmodelle); Fließgeschwindigkeit des Eises mit zeitlichen und saisonalen Änderungen; Deformationsbestimmung der Eisoberfläche und Strain-Analyse; Vergleich der Ergebnisse mit meteorologischen Daten und regionalen Klimamodellen; Validierung von Ergebnissen der Satelliten-Messungen aus ICESat (USA), CryoSat-2 (ESA); Operation IceBridge (USA) und TanDEM-X (ESA). Die Bestimmung von Höhenänderungen, Bewegungen und Deformationen erfolgt an zwei Untersuchungsgebieten: Swiss Camp (SWC, Breite = 69.6° Nord; Länge = 49.3° West, Meereshöhe 1170 m) südlich der alten EGIG-Linie, und ST2, 170 Meter niedriger gelegen und 15 km näher am Eisrand. Im Messgebiet SWC fanden seit 1991 bis 2014 insgesamt 12 Messkampagnen statt, im Durchschnitt also alle zwei Jahre. Bei ST2 begannen die Messungen 2004 und bis 2014 erfolgten hier 6 Kampagnen. Es handelt sich somit um eine Langzeitmessung, wie sie in ganz Grönland einmalig ist. Einen Bericht mit Stand 2006 geben Stober & Hepperle (2006). Die Höhe des Inlandeises hat bei SWC seit 1991 um 14.4 Meter abgenommen (entsprechend einer Massenabnahme von 13.0 m w.e.), wobei die Abnahme sich stark beschleunigte. Dieselbe Tendenz zeigte sich auch bei ST2. Die Höhenänderungen sind nicht konstant über die Messgebiete, sondern es zeigen sich ausgeprägte systematische lokale Unterschiede, deren Ursachen (z. B. Albedo, Feuchtigkeit u. a.) noch ungeklärt sind. Die Fließgeschwindigkeit verhält sich nicht einheitlich. Bei SWC fließt das Eis schneller als bei ST2 und während bei SWC eine Beschleunigung auftritt, zeigt sich bei ST2 eine Geschwindigkeitsabnahme, vermutlich wegen des aufsteigenden Randgebirges. Strain-Raten wurden für jedes Messgebiet über die meisten Epochen berechnet. Sie variieren jedoch stark und zeigen, dass der örtliche Untergrund des bewegten Messfeldes die Ergebnisse stark beeinflusst. Die Strainraten in Längsrichtung zwischen beiden Messgebieten sind negativ, was einer Stauchung (Kompression) des Eises entspricht, die zu einer positiven dynamisch bedingten Massenbilanz führt. Der Einfluss von einzelnen meteorologischen Parametern auf die Höhenänderungen wird mit einer Korrelationsanalyse untersucht. Allerdings gibt es selten signifikante Korrelationen, am deutlichsten und in beiden Messgebieten mit der sommerlichen Albedo. Weniger relevant erweisen sich die Lufttemperatur sowie die Nettostrahlung. Vergleiche der geodätischen Massenbilanz (GMB) mit der spezifischen Massenbilanz aus Pegelmessungen (SMB) ergeben abweichende Ergebnisse. Bei SWC beträgt die kumulierte GMB -13.0 m w.e. (2014), während SMB hier mit -10.1 m w.e. endet. Aus der Differenz GMB gegenüber SMB ergibt sich der dynamische Anteil. Dieser ist bei SWC und ST2 entgegengesetzt. Der dynamische Anteil wird zum Vergleich aus der vertikalen Strain-Komponente mittels der Kontinuitätsbedingung ermittelt. Die Übereinstimmung ist jedoch auf die anfänglichen Messjahre beschränkt. Ergebnisse von Satellitenmessverfahren werden mit Geländemodellen aus Bodenmessungen verglichen. Altimetrie mit ICESat von 2005 ergab Abweichungen in der Oberflächenhöhe (GPS – ICESat) im Mittel -0.13 ± 0.06 m. Vergleiche von Höhenänderungen aus CryoSat-2 zwischen 2011 und 2014 zeigen beträchtliche Unterschiede von 0.24 m/a (SWC) und 0.48 m/a (ST2). Höhen aus einem TanDEM-X Höhenmodell im August 2014 ergaben einen Offset vom GPS Geländemodell von 3.14 ±0.025 m. Die Standardabweichung eines Punktes liegt bei 1.07 m. Die Fließgeschwindigkeit aus verschiedenen Satellitenverfahren wird mit Bodenmessungen aus GPS verglichen. Daten aus den Jahren 2010-2017 von Sentinel-1 IW, TerraSAR-X, und ALOS PALSAR ergeben meist (Ausnahme PALSAR) recht gute Übereinstimmung innerhalb der Messgenauigkeit der Satellitenverfahren.

Keywords: Geodetic ground measurements, Elevation change, flow velocity, strain, mass balance

doi:10.2312/polarforschung.88.2.99

[1] Hochschule für Technik Stuttgart, [1] Stuttgart University of Applied Sciences
Manuskript eingereicht 3. April 2018; zum Druck angenommen 11. September 2018

1. INTRODUCTION

1.1 Geodetic measurements for Greenland ice sheet studies

The study of ice mass change is a central research topic within climate change. This study sets out to investigate the evolution of the latest mass balance, to determine whether the observed mass balance is in accordance with the models and how the models can be refined and calibrated. Principally, ice mass changes can be determined by several methods:

• Input-Output-Method: the sum of accumulation, melting (ablation) and iceberg calving. Accumulation and ablation are determined by the surface mass balance (SMB). The transfer of masses takes place via dynamical processes (ice flow and deformation).
• Satellite-gravimetry by GRACE. Changes in measured gravity show large-scale mass changes. The resolution in area is limited by ca. 200-300 km.
• Surface elevation observations by several methods:
- Combination of multi-sensor methods including stereo photogrammetry (e.g. SCHENK et al. 2014),
- by measured area-covering satellite altimetry,
- or by determination of surface elevation changes (dH/dt) measured by terrestrial geodetic methods. In addition, the elevation changes must be converted into mass changes by density values.

Geodetic long-term measurements on the ice surface are very laborious, logistically difficult and expensive. In contrast to satellite measurements, the geodetic ground measurements are more precise but can only be realized over limited areas and time. The result is a (local) mass balance with high accuracy, but representative of the research area only. They are mostly applied for single glaciers. On the Greenland ice sheet longer-lasting geodetic projects are rare.

Geodetic surface measurements were performed in Greenland during the international EGIG campaigns (EGIG = Expédition Glaciologique Internationale au Groenland) in a West-East profile across the ice sheet at a latitude of about 70°. Major aims were the determination of ice flow vector components (velocity, flow direction) and elevation change of the inland ice. The first EGIG campaigns were performed in 1959 and repeated in 1967/68, then later continued (1990/92) by scientists from the TU Braunschweig. The results along the EGIG line are presented by Möller (in HOMANN et al. 1996). On average, between 1959 and 1968 an elevation increase of about +0.10 to +0.15 m/a was obtained, but between 1968 and 1990 there was an elevation decrease of -0.20 to -0.30 m/a, especially in the western part of the EGIG line. No results were available from the EGIG line near the western ablation area, due to the lack of repeated measurements on identical points.

More recent geodetic measurements (GPS) were performed at Swiss Camp by ZWALLY et al. (2002). They derived the ice velocities from GPS-measured positions of a 4-m pole embedded two metres in the ice beginning in June 1996. They report seasonal variations of ice flow velocities caused by increased melting rates and faster sliding on the bedrock. These results have been confirmed by ice flow models in the latest publications (COLGAN et al. 2011a, b, c and 2012).

Further GPS-measurements were reported by KORTH et al. (2008) and KORTH et al. (2010). In an East-West profile along the historical route of DE QUERVAIN, elevation changes were determined between 2002, 2006, 2010 and, most recently, 2015. The results show a slight height increase in the central part (in the first years) and a large height decrease at the ice margins. JEZEK (2012) reports surface elevation and velocity changes on the south-central Greenland ice sheet between 1980 and 2011. In three clusters repeated GPS in situ observations were combined with airborne satellite measurements from ICESat.

Here we present long-term in situ geodetic observations conducted at two sites in West Greenland using terrestrial GNSS/GPS measurements. The scientific objectives are:
• Elevation changes of the ice surface at points (stake positions) distributed over the area.
• Determination of digital elevation models.
• Ice flow velocity with temporal and seasonal variation.
• Determination of the ice surface deformation (horizontal strain analysis).
• Comparison of results with meteorological data and regional climate models.
• Validation of satellite altimetry from ICESat (NASA), CryoSat-2 (ESA) and TanDEM-X (DLR).

1.2 Study sites

Swiss Camp is located on the inland ice (Latitude = 69.6° North; Longitude = 49.3° West, altitude 1170 m) south of the old EGIG line (Fig. 1) at a distance of 80 km from the coastal town Ilulissat (Jakobshavn/JAV). Swiss Camp was established in 1989 by the ETH Zürich and continued since 1992 by the University of Colorado at Boulder/USA (OHMURA et al. 2001; STEFFEN et al. 2006) in order to study climatology.

There are a number of particular glaciological reasons for the election of this research area at Swiss Camp:

• Catchment area of the Jakobshavn Isbrae Glacier;
• Situation and altitude near the equilibrium line (REEH 1989);
• Continuation of the EGIG-line towards the West coast;
• Terrestrial validation areas for remote sensing methods and satellite altimetry;
• Use of the camp site from ETH Zürich and the University of Colorado at Boulder/USA respectively as a logistic base.

At Swiss Camp the first geodetic measurements were performed in 1991 in connection with a project to study the influence of refraction over ice on height measurements by trigonometric and geometric levelling (STOBER 1995). This was continued in the following years as a project purely focused on deformation and elevation change for studies on climate change.

The author performed twelve campaigns between 1991 and 2014, thus on average every second year. This represents a unique, long-term project in all Greenland with precise geodetic ground measurements. In 2004 it was extended by a second measuring area called "ST2" (Latitude = 60.33° North; Longitude = 49.65° West, altitude 1000 m), situated at 170 metres lower elevation, in order to analyse the dependence on

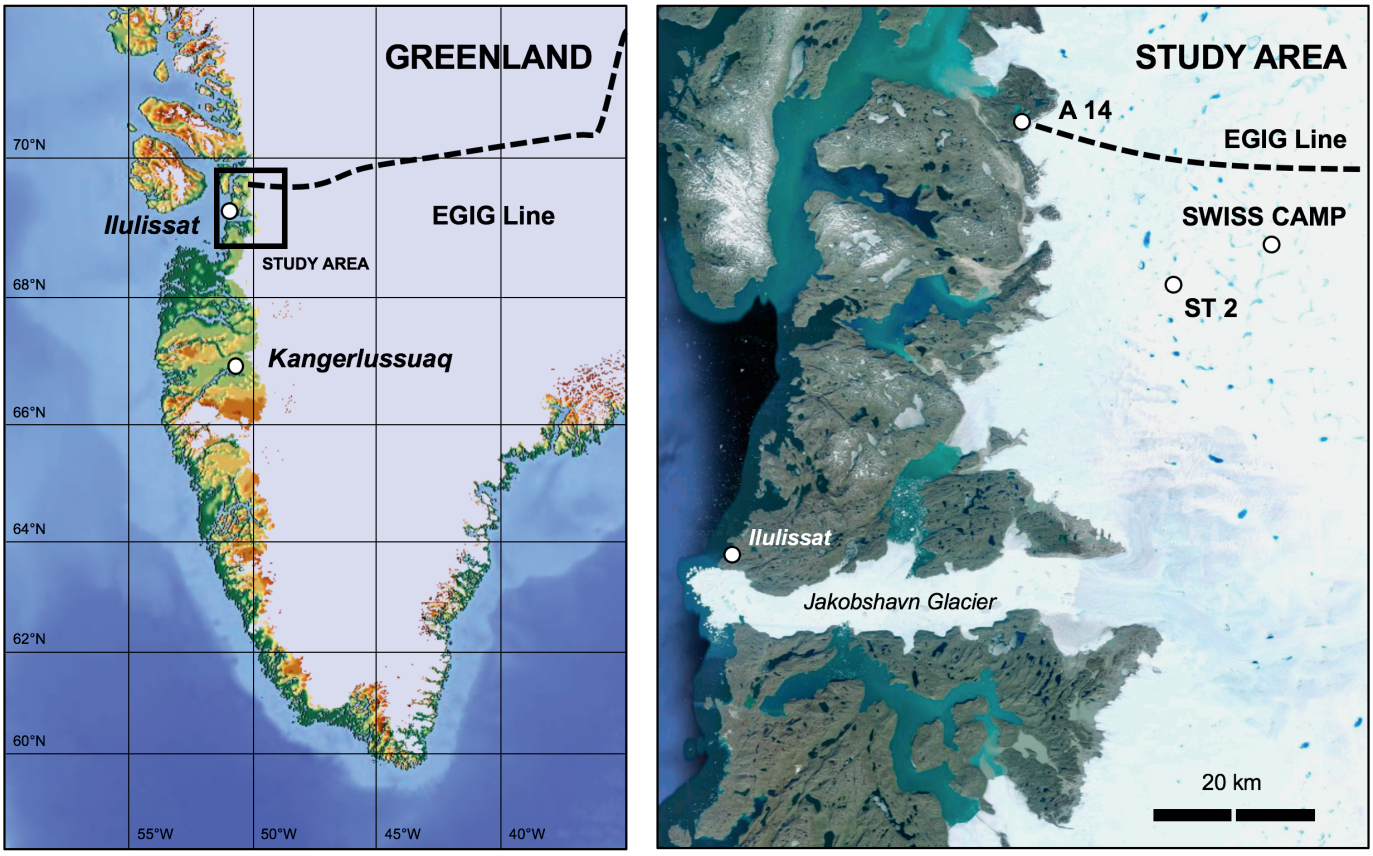

Fig. 1: Left map shows overview of the southern part of Greenland with the track of the IGIG Line and the small inset, indicating the location of the study area (topography from <www.maps-for-free.com>). The map to the right shows details of the study area in the northeastern Hinterland of Ilulissat and Jakobshavn Glacier (background image by LANDSAT 8 from google maps, 13. December 2018). It also shows the locations of the two study sites SWISS CAMP and ST 2 as well as the track of the EGIG Line.

Abb. 1: Die linke Karte zeigt einen Überblick über den südlichen Teil von Grönland mit dem Verlauf der EGIG-Linie. Das kleine Rechteck deutet auf die Lage des Arbeitsgebiets (Topographie von <www.maps-for-free.com>). Die Satellitenaufnahme auf der rechten Seite zeigt Details des Arbeitsgebiets nordöstlich von Ilulissat und dem Jakobshavn-Gletscher (Landsat-8-Szene von google maps, 13. Dezember 2018). Sie zeigt zudem die Untersuchungsstandorte SWISS CAMP und ST 2 sowie den Verlauf der IGIG-Linie.

altitude and distance to the ice margin. By 2014, 6 campaigns had been carried out in the area. Both measuring sites belong to the catchment area of the Jakobshavn Isbrae, which represents the draining by 6.5% of all Greenlandic ice masses (Weidick 1995). This part of Greenland is also referred to as the Paakitsoq area.

2. METHODS

2.1 Field measurements

In the research areas four aluminium stakes were drilled into the ice. They formed a triangle with a central point. At the coast in Ilulissat was a reference point on solid rock, EUREF-0112, which was determined in 1990 during the international EUREF-GPS campaign North-West (EUREF = The European Reference Frame for Georeferencing) in order to develop a world-wide network in the International Terrestrial Reference Frame (ITRF). For each campaign, a temporal reference station ("ice reference") was established on the ice surface near the research areas. Its coordinates were determined from differential static GPS measurements carried out simultaneously with measurements at EUREF-0112. The local GPS measurements in the research areas were attached to this ice reference and measured by static and kinematic GPS surveys with two-frequency-GPS-receivers (Systems Leica WM102, 300, 500 and 1200). More specifically, the following measuring programme was performed in all campaigns:

- Reference point in Ilulissat (EUREF-0112) on solid rock (and local backup network).
- Baseline Ilulissat (Jakobshavn, JAV) to ice reference in research areas (Swiss Camp 80 km, ST2 65 km) by static GPS, 6-8 hours.
- Current stake positions from ice reference to stakes by GPS static or Real-Time-Kinematik (RTK).
- Reconstruction/staking-out of the former stake positions from all previous campaigns (RTK-GPS). Fig. 2 (left) shows the situation of the moving stake network for all campaigns, 1991–2014.
- New measurement of current surface heights at all these previous stake positions.
- Measuring of the remaining snow cover in order to correct the heights to the ice horizon. Relevant to the situations 1991–2005.
- Topographical survey of ice surface around Swiss-Camp/ST2 with RTK-GPS with grid points every 100-200 metres

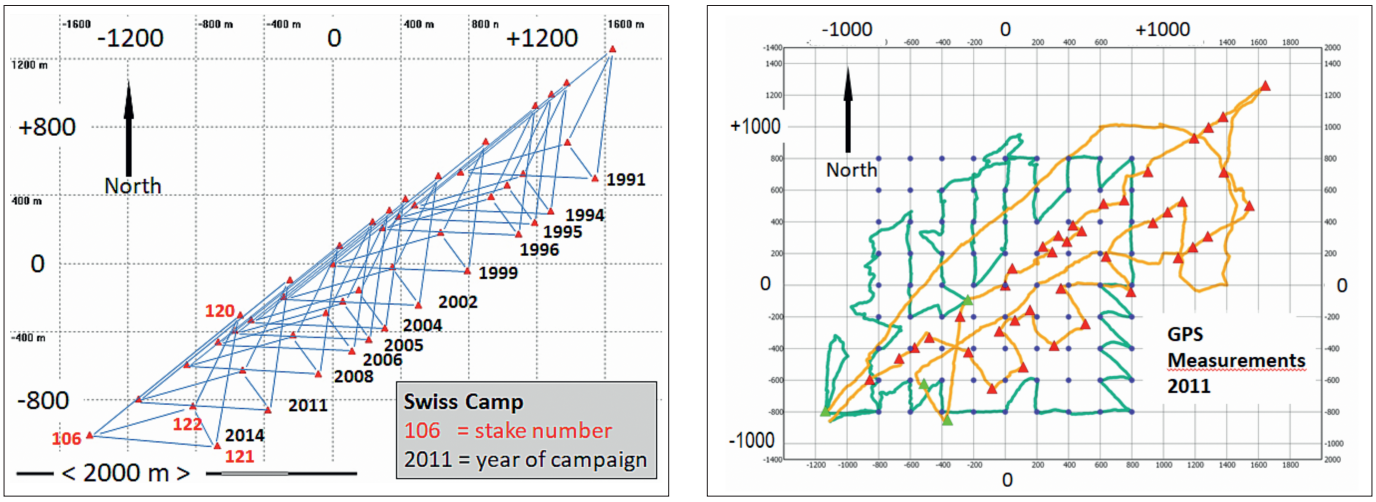

Fig. 2: (Left) Location of the 4 stakes (triangles with central point, marked with blue lines in the figure) moving with the ice from North-East to South-West at Swiss Camp (1991–2014). All previous stake positions were re-measured in the successive campaign. (Right) Pathways of all kinematically measured topographical points at Swiss Camp, example 2011. Two rover groups (green and yellow) measured the whole area by grid points, stake positions, and profiling along the pathways with steps of 5 seconds. GPS coordinates transformed into a plain cartesian coordinate system with its origin in stake 106 position 1999.

Abb. 2: (Links) Lage der 4 Pegel (Dreieck mit Zentralpunkt, gekennzeichnet durch blaue Linien) bei deren Wanderung mit der Eisbewegung von Nord-Ost nach Süd-West (1991-2014). (Rechts) Trassen aller kinematisch gemessener GPS-Punkte bei Swiss Camp, Beispiel 2011). Mit zwei Rover-Trupps (grün und gelb) wurde das gesamte Messgebiet über Gitterpunkte (Abstand 100-200 m) und Profile mit fünf Sekunden Zeitabstand gemessen. Die GPS Koordinaten (WGS84) wurden in ein lokales, ebenes kartesisches Koordinatensystem mit Nullpunkt in der Position 106/1999 transformiert.

and kinematic GPS profiling, area approximately 2 × 2 km^2. The mobile GPS receiver was transported on foot in a rucksack. During the walk the signal to the reference station was permanently maintained. Therefore, the GPS carrier phase ambiguity solved at the starting position was transported all over the terrain (baselines 2-3 km) and maintained for all measured profiles and all grid points. Fig. 2 (right) shows the pathways for the topographical measurements at Swiss Camp 2011 as an example.

- Reading of free stake length over snow or ice in order to determine the specific mass balance (SMB) at stakes (since 1991).

At both survey areas the heights of all previous stake positions were re-measured in every campaign. All geodetic elevation measurements were referred to the ice horizon. If there was any remaining snow cover, this was measured and the heights corrected accordingly. Substantial snow cover was present in 1991 (0.62 m), 1994 (1.46 m), and 1995 (0.69 m). Slight snow cover existed during the campaigns 1996–2005 (≤ 0.2 m), while in subsequent years the winter snow had melted by the time any measurements were taken. In the evaluation height comparisons between different epochs were calculated.
Two methods were applied:

- Height comparison at identical (previous) stake positions. Given that we always compared the heights at identical (previous) stake positions (Eulerian reference system), the derived elevation changes were not affected by terrain slope.
- Height comparison between Digital Elevation Models (DEM) over the whole area. The DEMs were based on all measured points (stake positions, grid points, kinematically measured profiles) in each campaign. Therefore, the points were unregularly distributed. To approximate a smoothed terrain surface, we used the software SURFER with the kriging method.

The ice flow was evaluated by the horizontal displacements of the stakes between successive campaigns.

2.2 Accuracy assessment of the discrete GPS point measurements

The general conditions for GPS in high latitudes (70°) were limited by: Bad satellite geometry due to no satellites in the zenith (elevation angle max = 70°) and influences by the ionosphere and troposphere due to longer pathways through layers. Typically 10-12 satellites were available with an elevation angle between 10° and 65° and with a GDOP (geometric dilution of precision) of between 2 and 4. GDOP is a term used in satellite navigation to specify the additional multiplicative effect of navigation satellite geometry on positional measurement precision. The smaller the value, the better the satellite geometry. The accuracy of the measured heights for discrete current and previous stake positions was dependent on:

- The accuracy of the GPS baseline JAV – ice reference (σ_B), (80 km long for Swiss Camp, 65 km long for ST2);
- local close-range GPS accuracy in the research area;
- the accuracy of setting out the previous stake positions;
- influence of local terrain inclination;
- definition of the ice surface.

The baseline JAV-ice reference was measured for 6-8 hours. After post-processing the standard deviation in height could be assessed by $\sigma_B \approx 3$ cm. Processing with different GPS-software (Leica SKI-Pro, Bernese Software) showed discrepancies of 5 cm in length and in height (Heise 2005). In order to obtain better comparability of all campaigns the Leica solution was always used for the final results. The local GPS-measurements at stakes were carried out with carbon poles by real-time-kinematic GPS (RTK) or in static method. Here the baselines were short (< 3 km). With usually solved ambiguities the differential position accuracy (σ_{RTK}) could be assessed by $\sigma_{RTK} = 2$ cm.

The staking-out of previous positions was also performed by RTK. However, at the time of measurement in the field, the

ice reference was only determined by a 20-minute single-point solution leading to a horizontal uncertainty of a maximum of 3 m. Only after post-processing were the exact coordinates available. Compared to the desired coordinates we obtained a discrepancy of ca. 1 metre on average. Due to the local terrain inclination of about 1-2 %, this position error gives rise to a height error σ_L = 2 cm. The mentioned independent error components result in a total height error of:

$$\sigma_{H0} = \sqrt{(\sigma_B^2 + \sigma_{RTK}^2 + \sigma_L^2)} = 4.1 \text{ cm} \qquad (2.1)$$

in every campaign. The standard deviation of a calculated height difference between two campaigns (σ_{HK}) is augmented by factor $\sqrt{2}$ (error propagation law), hence σ_{HK} = 5.7 cm. These accuracy assessments are confirmed by an error analysis of the elevation changes between the different stakes (see section 3.1, Fig. 5). Furthermore, it was necessary to consider the definition of the local ice surface. At Swiss Camp this was smoother than at ST2, but a local waviness of 10 cm was always possible, in exceptional cases up to 0.5 m. These irregularities could only be adjusted by the large number of measured points.

2.3 Assessment of the accuracy of topographical measurements

The accuracy of the measured topographical points was almost the same as for the stake positions because we used the same RTK-GPS method. Further, the profiles measured by walking were usually performed with solved ambiguities. The distance between measured points varied between a few metres (profiling) and a maximum of 200 metres (grid). All points were used to calculate the Digital Elevation Model (DEM) with the software SURFER.

The accuracy of the derived DEMs is difficult to assess, however. Given the irregular distribution of measured points (some parts consisted of more or sparsely measured data points), the surface model was generalized with an unequal smoothing effect. But no topographic structures such as edges or sudden deep valleys exist in these study areas. So the smoothed model represents the surface precisely enough for comparisons to be made between campaigns.

3. RESULTS

3.1 Elevation changes at stakes

The annual movement of the stakes amounted to about 115 metres (at SWC). The heights of the current position and all previous positions were measured in all successive campaigns. The oldest position (1991) was therefore re-measured most frequently, whereas the second to last measurement (2011) was repeated only once. Consequently, a history of elevation changes can be formed for every stake. As an example, we show in Fig. 3 the elevation development of Stake 121 at Swiss Camp.

The average cumulative elevation change for all stake positions at Swiss Camp (1991–2014) and ST2 (2004–2014) are shown in Fig. 4. In addition to our project, in summer 2015 KORTH re-measured the heights of a few points (therefore

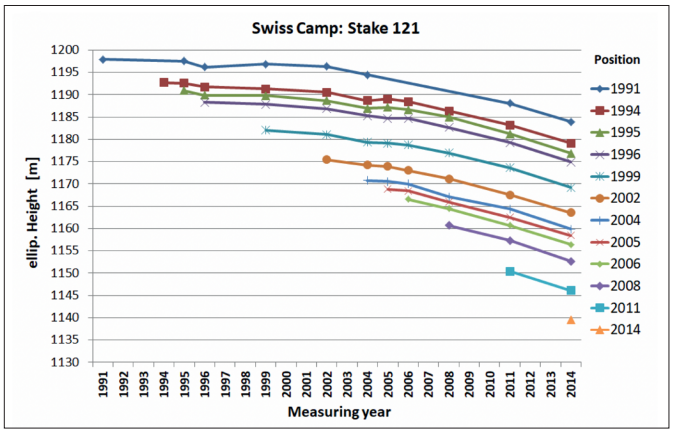

Fig. 3: Swiss Camp, Stake 121: Elevation development of the ice horizon 1991–2014. The curves in a horizontal direction show the elevation as being at the very same position in the different measuring years. E.g. the uppermost line (blue) shows the height development at the very same position (1991), the second line (red-brown) corresponds to the successive positions (1994) and so on. Already here we detect an accelerated elevation loss in recent years. In the vertical direction the curves show the height change of a distinct position in the consecutive campaigns. The connection of the first dots in each horizontal row indicates the height change as a result of the terrain inclination along the flow line of this stake (longitudinal section along the flow line). The graph shows the consistency of all the results.

Abb. 3: Höhenentwicklung des Eishorizonts 1991-2014 von Swiss Camp, Pegel 121. Die Kurven in horizontaler Richtung zeigen die Höhen an der genau gleichen Position in den verschiedenen Messjahren. Beispielsweise zeigt die oberste Linie (blau) die Höhenentwicklung für die Position des Pegels 121 im Jahr 1991. Die zweite Linie (rot-braun) dann entsprechend für die Position desselben Pegels im Jahr 1994, usw. Bereits hieraus wird die beschleunigte Höhenabnahme im Lauf der Jahre erkennbar. In vertikaler Betrachtungsweise zeigt die Höhe des wandernden Pegels in allen folgenden Kampagnen. Die Verbindungslinie aller ersten Punkte der horizontalen Kurven ergibt die Geländeneigung entlang der Fließlinie (Längsprofil) des Pegels 121. Die Graphik zeigt die Konsistenz aller Resultate.

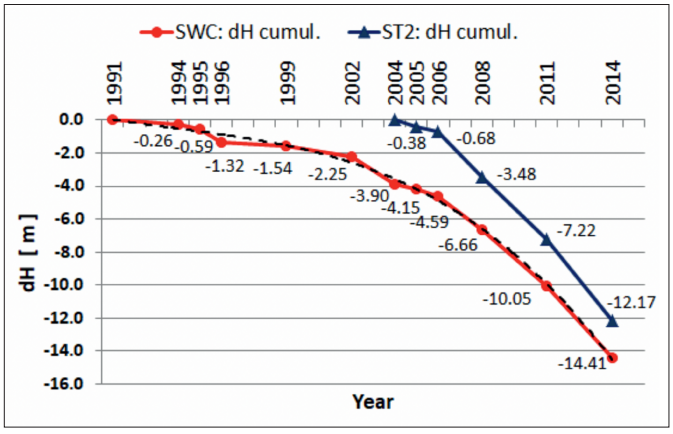

Fig. 4: Cumulative elevation change of the ice surface at Swiss Camp, 1991–2014 (red), and at ST2, 2004–2014, (blue). The elevation changes, comparable since 2004, indicate a similar elevation decrease, but which are even more pronounced at the lower-situated site at ST2. The cumulated standard deviations at SWC range from 0.25 (1995) to 0.35 m (2014), and at ST2 to 0.16 m (2014).

Abb. 4: Kumulierte Höhenänderung bei Swiss Camp, 1991-2014, (rot) und bei ST2, 2004-2014, (blau). Die Höhenänderungen, vergleichbar ab 2004, ergeben eine ähnliche Höhenabnahme, jedoch verstärkt bei dem tiefer gelegenen Messgebiet ST2. Die kumulierten Standardabweichungen bei SWC liegen bei 0.15 (1995) bis 0.35 (2014), und bei ST2 bei 0.16 m (2014).

minor accuracy) in the stake profile 106 (SWC). Here we obtained an elevation change for 2015–2014 of -0.99 ±0.15 m/a (KORTH, personal communication 2015, not included in Fig. 4). This is less than in the previous years (2014–2011:

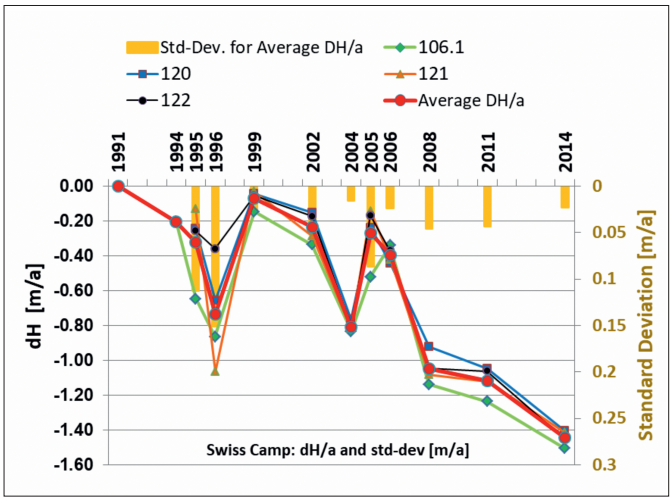

Fig. 5: Elevation changes per year at stake positions and on average for all stakes and their standard deviation (yellow) in the Swiss Camp area.

Abb. 5: Höhenänderungen pro Jahr für jeden einzelnen Pegel und im Mittel aller Pegel mit Standardabweichungen (gelb) im Gebiet Swiss Camp.

-1.45 per year), and consistent with the relatively cold summer of 2015. The long-term development at SWC is indicated by the smoothed polynomial curve (Fig. 4, dotted curve). It shows an accelerated elevation decrease, especially in the last warm years. The analogous results for ST2 show the same increased elevation change since 2006.

The elevation changes for every distinct stake, and on average for all stakes (Fig. 5), vary significantly from year to year. Small dH/a appear between 1999–1996, 2002–1999, and 2005–2004, large ones between 1996–1995 and 2004–2002, and for all years since 2008.

The accuracy of elevation and elevation change achieved in reality can be derived by using the differences of the elevation changes per year (dH/a) for every distinct stake and on average over all stakes between all campaigns (Fig. 5). The elevation change variation between the 4 stakes is indicated by the standard deviation (σ_1) for the average dH/a (yellow balks). It is largest for 1996–1995 (σ_1 = 0.15 m/a) followed by 1995–1994 (σ_1 = 0.11m/a) and 2005–2004 (σ_1 = 0.09 m/a). For the rest it is in the order of 0.05 to 0.02 m/a. The t-test (t = dH/σ_1) was applied to test for significance. Except for earlier years (1995–1994 and 1999–1996), all values are over 3 up to 60, meaning the elevation changes are significant. In sum, we can conclude that the elevation changes from stakes are precise in the expected order of measuring accuracy (ca. 0.06 m/a, cf 2.2) and that they are statistically significant.

3.2 Elevation changes from topographical surveys

The topography of both areas is significantly different. Whereas Swiss Camp (at an altitude between 1150 and 1190 m) is inclined almost uniformly (1.8 %), ST2 (at an altitude between 970 and 1010 m) is much more shaped by a crest in a South-West direction. Fig. 6 shows typical digital elevation models for both of our measuring areas, Swiss Camp and ST2.

The difference between the digital elevation models (DEM) of the two consecutive campaigns gives the volume change and the mean elevation change over the area. On average the results agree with those from stake positions (Section 3.1) within the limits of the measuring accuracy (Section 2.2). As an example, Fig. 7 (left) shows the difference between the digital elevation models 2011 and 2014 at Swiss Camp. Between the campaigns 2011/2014 we obtain here a mean elevation change of -4.41 m or a rate of -1.47 m per year in accordance with the result of stake positions (-4.37 m and 1.46 m/a respectively).

Systematic local smaller and larger variations of elevation changes are remarkable, so-called “regional effects”. Between 2011 and 2014 the elevation changes varied in a wide range over the whole area. We obtained elevation changes from -6.0 to -1.6 m at ST2 and -5.2 to -3.9 m at SWC. Obviously, there are parts with more and less elevation change. The vari-

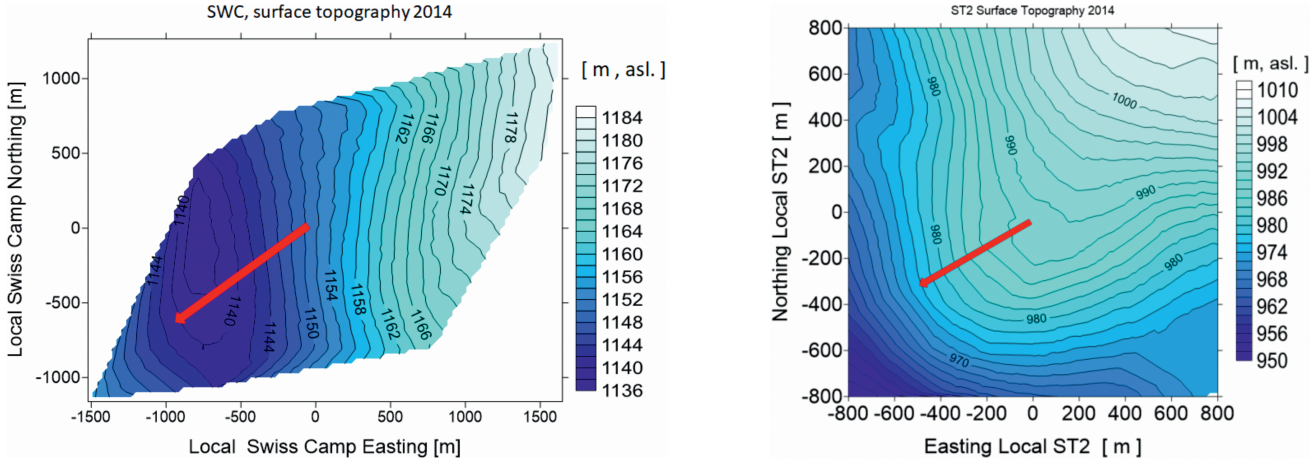

Fig. 6: The topography of the areas Swiss Camp (left) and ST2 (right) and ice flow direction (red arrow) in 2014. The topographical measurements and surface interpolation using the SURFER program are based on grid points every 200 metres and densification by profiling between GPS grid and stake positions. An example for the pathways with distribution of used points at SWC 2011 is shown in Fig. 2, right.

Abb. 6: Topographie der Gebiete Swiss Camp (links) sowie ST2 (rechts) mit Fließrichtung des Eises. Die topographische Aufnahme beruht auf Gitterpunkten im Abstand von 200 Meter und Verdichtung mittels GPS-Profilen zwischen den Gitter- und Pegelpositionen. Das interpolierte Oberflächengeländemodell wurde mit dem Programm SURFER erstellt. Ein Beispiel für die zur Messung verwendeten Daten zeigt Abb. 2, rechts.

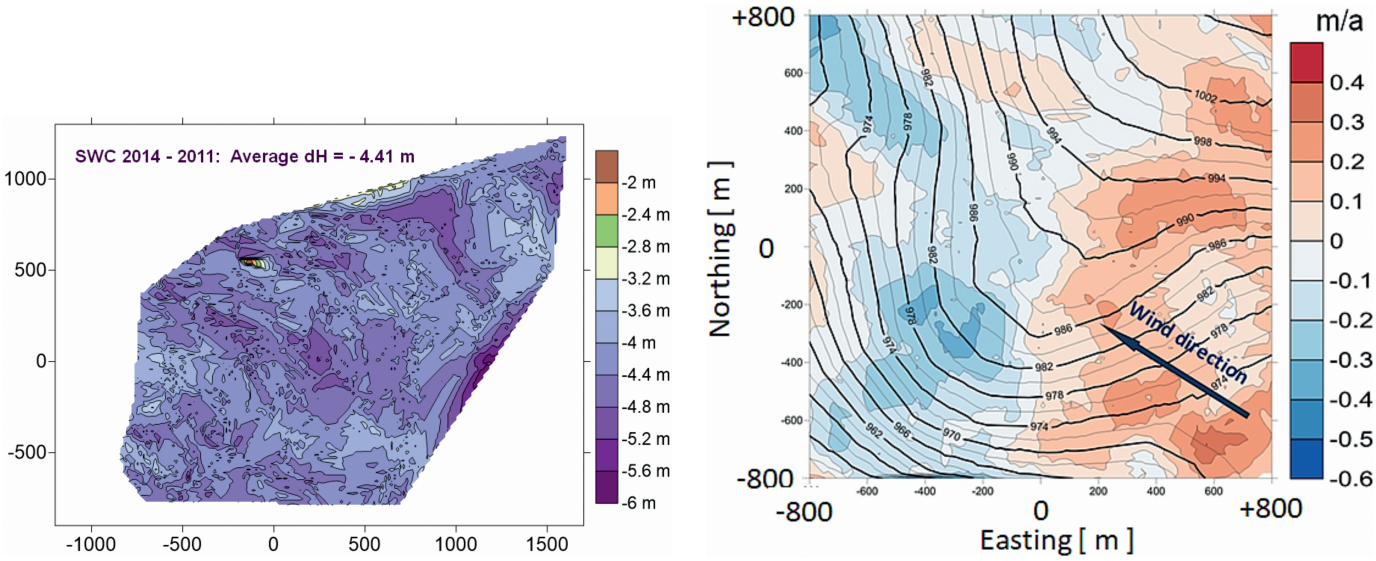

Fig. 7: (Left) Average elevation change -4.41 m at Swiss Camp derived from digital elevation model differences 2014–2011. (Right) Residual local elevation change rates ("regional effects"), reduced by the mean annual elevation change -1.41 m/a at ST2, 2014–2008. Similar effects appear in many consecutive campaigns. This appears to signify systematic behaviour.

Abb. 7: (Links) Durchschnittliche Höhenänderung -4.41 m bei Swiss Camp aus Differenzierung von digitalen Höhenmodellen 2014-2011. (Rechts) Residuen lokaler Höhenänderungen („Lokaleffekte") nach Reduktion um die mittlere jährliche Höhenänderung -1.41 m/a bei ST2, 2014-2011. Ähnliche Effekte ergeben sich zwischen vielen weiteren Kampagnen, die somit auf eine Systematik hinweisen.

ations do not seem to be accidental, because a detailed study with difference digital elevation models from older periods show a similar local systematic variability. After reduction of the mean elevation change of the whole area, the remaining residual elevation changes show the local discrepancies. An example is given for ST2 2014–2008 (Fig. 7, right). Parts with more or less elevation change are clearly visible. This result also regularly trends in other years. As another example, the measured local variations in elevation change for ST2, 2005–2004, were analysed. The height changes at 64 grid points (distance every 200 m) differ on average by -0.38±0.06 m/a. Here also, it is possible to distinguish parts with more or less elevation change.
Possible reasons for local elevation change variations are:

- Solar radiation in relation to topography (terrain inclination);
- surface condition, water content;
- albedo (luminosity, reflectivity);
- relocation of accumulated snow by wind;
- apparent elevation change by moving topographical structures (crest, valley);
- further causes, such as additional interpolation artefacts by the DEM filtering (less probable because point distribution is mostly the same).

We can exclude moving topographical structures. Crest and valley remain constant at the same places. In Fig. 7 the regional effects at ST2 are shown together with contour lines, and wind direction. The prevailing wind direction is from the South-East (data GC-Net) and would blow snow from this part over the crest, which stretches along the NE-SW direction. The daily net radiation is dominated by the daily sun course and the local albedo. Small-scale spatial albedo variations may occur on glacier ice and cause large spatial differences in ablation (VAN DE WAL et al. 1992; KONZELMANN & BRAITHWAITE 1995; HOCK 2005). A locally-reduced albedo is also caused by cryoconite holes on the glacier surface. They are filled with dark-coloured materials that consist of dust, mineral powder and micro-organisms. The most recent research (RYAN et al. 2018) confirms this theory. At ST2 we found many surface waves and sastrugi of up to 1 metre, especially in the South-Eastern part, where anomalous surface reflection is possible. This seems to be confirmed by a first luminosity measurement by simple photographs of the snow/ice surface (HÖNES 2015; STOBER 2016). The melt due to sun-exposed parts by terrain inclination and sun direction is dominated by the NE-SW ridge dividing the terrain in more and less melt-sensible parts. In addition, specific hydrological conditions due to water content, also in the underground, seem probable, where rapid drainage most often occurs in the ablation areas during summer periods HOFFMANN et al. 2011; MORRISS et al. 2013). Given the local variation, the accuracy of the DEM differencing is difficult to assess.

We examined the elevation changes from in both years measured grid points, without interpolation. At ST2, 2014–2008, there were 53 comparable grid points with spacing 200 metres. On average the heights differed by -1.37±0.02 m/a. The visualization of the height changes reduced by the mean is depicted in Fig. 8, left. The same data was used for construction a DEM with the SURFER program and application of the kriging method (Fig. 8, right). It clearly shows the same characteristics with local different dh/dt and proves the kriging interpolation method, which did not produce artefacts due to interpolation errors. The residuals also agree with the dh/dt DEM Fig. 7 (right), constructed with full data (containing kinematic profiling between stakes).

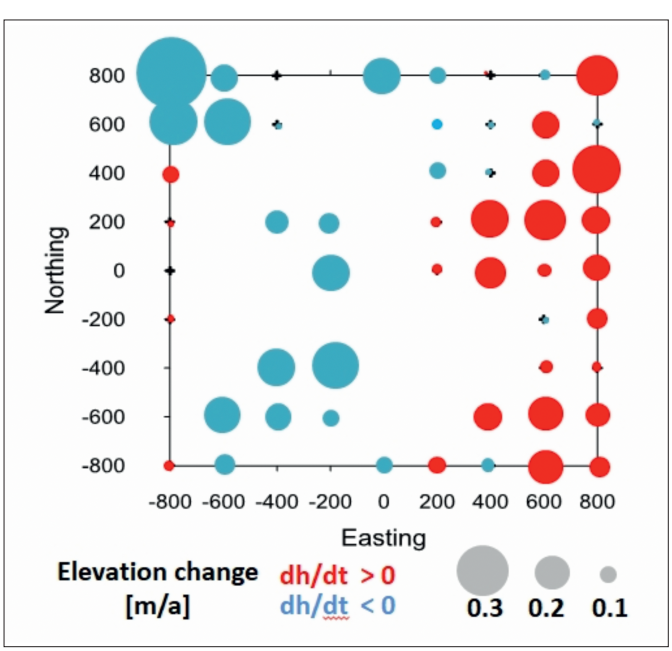

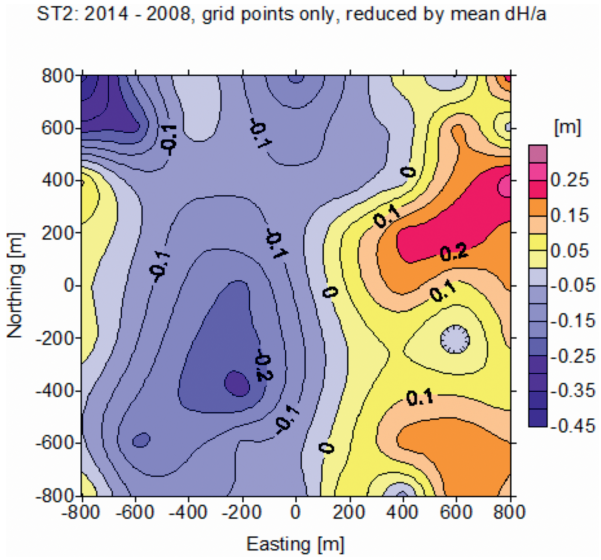

Fig. 8: (Left) Residual elevation changes at ST2, 2014–2008, using grid points with spacing 200 m only. Not every grid point could be measured in both campaigns. (Right) Elevation change model constructed with the Surfer kriging method using the same grid points only.

Abb. 8: (Links) Residuen von Höhenänderungen bei ST2, 2014-2011, bei ausschließlicher Verwendung von direkt wiederholt gemessenen Gitterpunkten im Abstand von 200 m. Nicht in beiden Kampagnen konnte jeder Gitterpunkt gemessen werden. (Rechts) Höhenänderungsmodell mittels der Surfer Kriging Methode bei ausschließlicher Verwendung dieser identischen Gitterpunkte.

3.3 Surface velocity

The ice flow vector (velocity and azimuth) was determined by comparing stake positions (horizontal coordinates) in different years measured by GPS (static or RTK). As a result, we calculated the horizontal displacements on average from all the available stakes. Small differences between the stakes appear, depending on the local topography. The average flow velocity and standard deviation e.g. 2011-2014 at Swiss Camp is (0.3264 ± 0.0017) m/d.

Both research areas, Swiss Camp and ST2, were found to behave differently and even contrarily as regards ice movement (Fig. 9). At SWC the mean flow velocity is 0.32 m/d, at ST2 the ice moves slower at 0.19 m/d. Temporal changes also differ. At SWC we found continuously increasing values. The speed here accelerates in a linear trend of +0.0008 m/d per year or +0.25% per year, and which increases according to a second order polynomial. At ST2 we found a deceleration by 0.0015 m/d per year or -0.77% per year.

In order to investigate seasonal summer ice flow velocities, we applied the GPS evaluation method Precise Point Positioning (PPP) in the kinematic mode (Zumberge et al. 1997; Kouba 2000; Mireault et al. 2008; Kettemann 2011; Giese et al. 2011; Rizos et al. 2012). We used the free on-line service from the Natural Resources Canada (NRCan) with the Canadian Spatial Reference System CSRS (www.geod.nrcan.gc.ca). The evaluation of the kinematically GPS data was split into a Northing and an Easting component, both with determination of adjusted linear straight lines and combination to amount and azimuth of movement. The accuracy of these straight lines provides a measure for PPP precision. On average it was

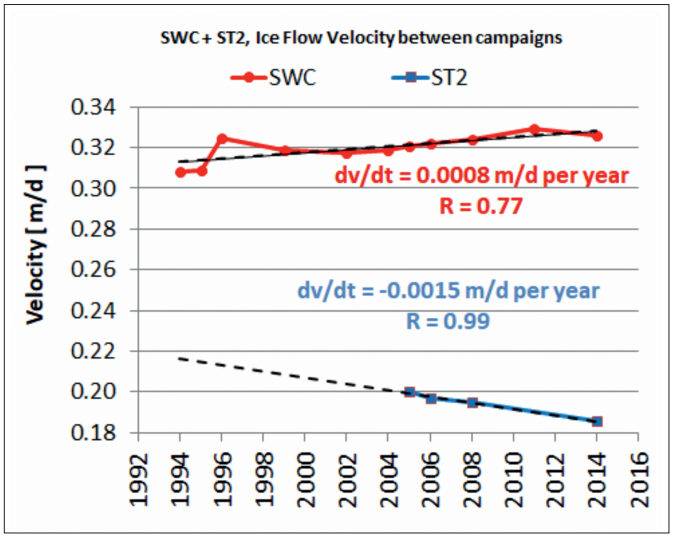

Fig. 9: Mean ice flow velocities at SWC (at top) and at ST2 (at bottom). In the period 2011–2014 at SWC the flow azimuth is 260.23 ± 0.31 gon. Over the whole period of observation slight variations were caused by topography and bedrock. The corresponding values for ST2 are 268.03 ±0.4 gon.

Abb. 9: Durchschnittliche Fließgeschwindigkeiten bei SWC (oben) und bei ST2 (unten). Im Zeitraum 2011-2014 beträgt bei SWC die Fließrichtung 260.23 ± 0.31 gon. Über die gesamte Beobachtungsdauer variiert sie leicht, verursacht durch die Topographie der Oberfläche und des Untergrunds.

assessed to ±0.03 m/d. Main error sources were the constellation of the satellites, and scintillation of the GPS signal due to tropospheric and ionospheric effects. The results of several campaigns with PPP are presented in Fig. 10. In comparison to the long-term average (SWC: 0.32 m/a, ST2: 0.19 m/a), the summer flow velocity is for the most part signifi-

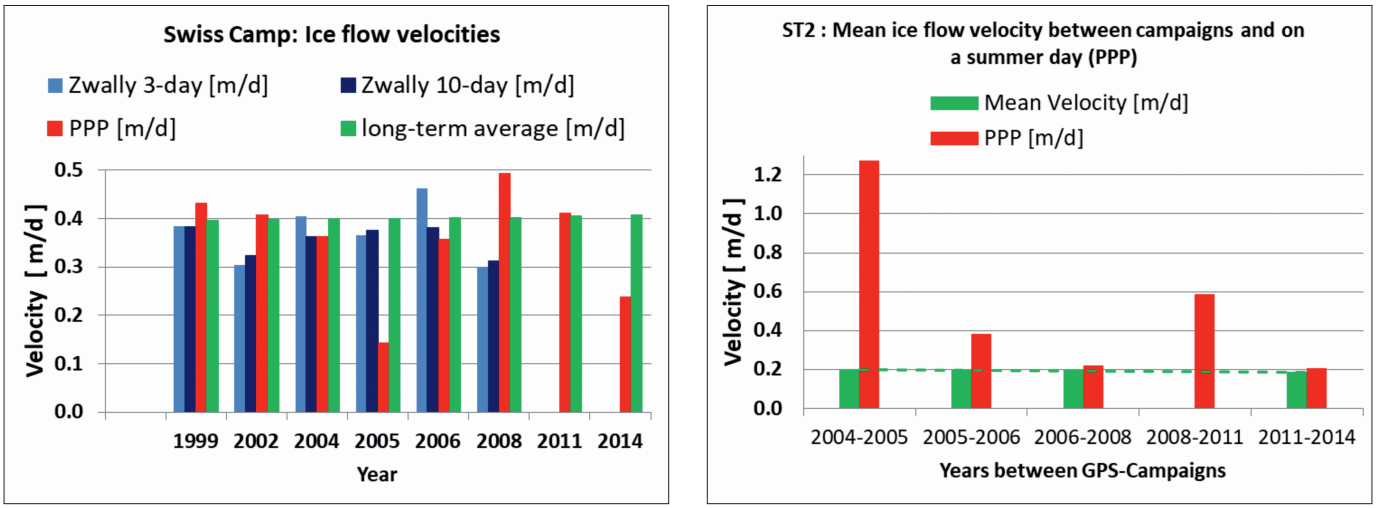

Fig. 10: Ice flow velocities in summer (red) at Swiss Camp (left) and at ST2 (right). SWC contains our long-term annual velocities (green) and the summer velocities from 3-days- and 10-days-averages (blue) from ZWALLY. At ST2 the annual average (green) deceleration is compared to the summer velocities (red). The accuracy of PPP was assessed to ±0.03 m/d.

Abb. 10: Fließgeschwindigkeit im Sommer (rot) bei Swiss Camp (links) und bei ST2 (rechts). Bei SWC sind neben den langzeitlichen Werten (grün) auch 3-Tages- und 10-Tages-Mittel von ZWALLY enthalten (hell- bzw. dunkelblau). Bei ST2 wird die langzeitliche Geschwindigkeitsabnahme (grün) mit den sommerlichen Geschwindigkeiten (rot) aus PPP verglichen. Die Genauigkeit von PPP wird zu ±0.03 m/d abgeschätzt.

cantly faster (with the exception of 2005 and 2014). These results correspond to observations (1999–2008) from Zwally at SWC (COLGAN et al. 2012, dataset ZWALLY pers. com.). Large discrepancies versus PPP appeared in 2005 and 2008. Zwally's 3- or 10-days averages contain more data than our 8-hour datasets, meaning short-term sudden movements such as relaxation or retardation caused by the bedrock or crevasses were possible.

3.4 Deformation and strain

The methodology of strain determination is based on the horizontal coordinates of the moving stake network. The relative length change ΔD/D of a distance D between two epochs 1 and 0 is given by

$$\Delta D/D = (D_1 - D_0)/D_0. \qquad (3.1)$$

Divided by the time interval (t_1–t_0) this gives the strain rate, often expressed in dimension ppm/year [ppm/a].
The differential deformation of the stake network consisting of four stakes (triangle with central point) was used for the strain analysis. The deformation and the strain parameters were determined by an affine transformation between two successive campaigns. An affine transformation is exactly determined by 3 points (horizontal coordinates x,y). In the case of the project there were 4 points, which created an over-determined system. This was solved by a least squares adjustment. As result we obtained the principal strain rates, extreme distortions (e_1, e_2) of the strain ellipse and their standard deviations, and the azimuth Θ of e_1. The formulas go back to WELSCH (1982) and they are presented in STOBER (2001). The main resulting parameters are principal strain rates in the direction of extreme distortions:

e_1 = principal strain rate in azimuth Θ, amount per year, [ppm/a]

e_2 = principal strain rate perpendicular to e_1 [ppm/a]
Θ = azimuth of e_1 [gon]

Applying the incompressibility condition of ice, the sum of all deformations in all three dimensions are given by

$$e_1 + e_2 + e_3 = 0 \qquad (3.2)$$

Hence the vertical strain component e_3 follows from

$$e_3 = -(e_1 + e_2) \qquad (3.3)$$

Using a MATLAB program, the following results were obtained. The vertical displacement of the ice surface due to horizontal strain in the vertical ice column can be assessed by

$$dH_e = e_3 * H * F \qquad (3.4)$$

where H = ice thickness, and F is a parameter to incorporate the depth dependent ice flow velocity with the assumption that the depth dependent strain will vary in the same manner as the ice flow velocity (STOBER 2001; STOBER 2008). The formulas are based on the ice flow law (PATERSON 1994; HOOKE 1998). The parameter F is a shape factor used to reduce the surface values (ice flow, strain rates) to the average values in the ice column with thickness H. The shape factors were determined as F = 0.93 (SWC) resp. F = 0.995 (ST2).

Swiss Camp	e1	e2	Azimuth e1	e_flow-line 260.5 gon	σ e1,2	t1= e1/σe	t2= e2/σe	e3 = = -(e1+e2)	dHe
Campaign	(ppm/a)	(ppm/a)	[gon]	(ppm/a)	(ppm/a)			(ppm/a)	(m/a)
1995–1994	900	-896	29.169	499	1001	0.89	-0.89	-4	0.00
1996–1995	*961*	-879	*24.937*	*444*	*251*	***3.83***	***-3.5***	***-82***	***-0.09***
1999–1996	*1215*	*-889*	*20.692*	*494*	*74*	***16.51***	***-12.08***	***-325***	***-0.35***
2002–1999	*1221*	*-903*	*13.46*	258	*223*	***5.49***	***-4.06***	***-318***	***-0.35***
2004–2002	403	-1714	-3.006	-1091	214	1.88	***-8***	1311	1.43
2005–2004	275	-4767	27.136	-988	2190	0.13	-2.18	4492	4.89
2006–2005	2669	-1557	-1.033	-193	804	***3.31***	-1.93	-1112	-1.21
2008–2006	-1404	-7813	17.517	-3908	2246	-0.63	***-3.49***	9217	10.03
2011–2008	757	-5737	9.188	-2624	832	0.91	***-6.9***	4980	5.42
2014–2011	*2985*	*-3760*	*-4.938*	*-1960*	*531*	***5.63***	***-7.09***	***775***	***0.84***

Tab. 1: Strain rates (e_1, e_2, e_3) and standard deviations (σ) at Swiss Camp. Dynamic component dH_e (m/a) for settings ice thickness H = 1170 m, shape factor F = 0.93. Significance (bold) starting from t > 3. Years with high significance in both axes (e_1 and e_2) are marked in bold italic numbers. The azimuth is given for e_1.

Tab. 1: Strainraten (e_1, e_2, e_3) und ihre Standardabweichungen (σ) bei Swiss Camp. Dynamische Komponente dH_e (m/a) für Werte Eisdicke H = 1170 m, Formfaktor F = 0.93. Signifikanz (fett) ab t > 3. Jahre mit hoher Signifikanz in beiden Achsen (e_1 und e_2) sind fett kursiv markiert. Das Azimut ist für e_1 angegeben.

3.4.1 Results, Strain rates at SWC and ST2:

The principal strain rates at Swiss Camp are summarized in Table 1 and in Figs. 11 a, b.
Table 1 shows the principal strain rates e_1, e_2, and the strain rate in the ice flow direction between successive campaigns together with their standard deviations. In addition, it contains the vertical component $e_3 = -(e_1+e_2)$ and the vertical surface change due to the strain rates.
In the flow line positive distortions (dilatation) appear in the azimuth from ca. 0-30 gon (e_1). In the perpendicular direction (e_2), negative distortions appear (compression). The directions of dilatation and compression remain almost constant, but the amounts vary considerably according to the year. Therefore, in Fig. 11a the values are smoothed by a running average over 3 campaign pairs, making the long-term trend of the strain rates clearly visible. Since 2005, and especially in more recent times, the amount of compression has increased significantly. High significance in both axes is given for 1996-95, 1999-96, 2002-1999 and 2014-2011. The negative values of the vertical component $e_3 = -(e_1+ e_2)$ increased between 1995 and 2002, and changed to positive values in the last campaigns between 2008 and 2014. For 2011-2014 and with the application of (3.4) and an ice thickness H = 1170 m (DTU 2005; Bamber et al. 2013) at Swiss Camp, we obtain a positive dynamic elevation increase of dH_e = +0.84 m/a. This corresponds to a virtual mass increase (density = 0.9) of dM_e = +0.76 m w.e./a. "Virtual" means that, in reality, height has changed despite the fact that no mass change has occurred (due to the incompressibility condition).

At ST2 the principal strain rates are very constant in algebraic sign with little variation in amount (Table 2, Fig. 11c, d). The component e1 is mostly significant ($t_1 = e_1/\sigma e \geq 3$), e_2 never. The vertical strain rate component e3 is negative, with a tendency towards decreased rates. With application of the (3.4) and an ice thickness H = 600 m (DTU 2005; Bamber et al. 2013) this signifies a negative dynamic elevation change dH_e = -1.42 m/a, corresponding to a virtual mass decrease (density = 0.9) of dM_e = -1.28 m w.e. per year. Hereby the depth dependent flow parameter F_{ST2} = 0.995 is negligible.

3.4.2 Longitudinal strain rates between SWC and ST2

The networks SWC and ST2 were approximately placed in the ice flow direction. The longitudinal strain rates were derived from the distortion of the distances between the stakes of both networks. Each network consisted of 4 stakes, which could be compared pairwise. On average, the distortions of the 4 distances between the campaigns were -2911 and -3446 ppm/a with standard deviations 25 to 74 ppm/a, thus with high significance. The distances (ca. 14.7 km) between SWC and ST2 were shortened on average by 3180 ppm/a or 46.8 m/a. Both networks SWC and ST2 approached each other.

The summarizing behaviour of ice flow velocity and strain rates (2011–2014) in our survey sites is shown together with the topography in the Paakitsoq region (data DTU 2005) in Fig. 12: The ice flows in the direction of the main downhill gradient of the terrain. The principal strain rates seldom agree with the ice flow direction. In general, in the flow azimuth we found compression, and perpendicular extension. This agrees with the longitudinal strain rate between SWC and ST2. Especially in the marginal region at ST2, the lateral distortion exceeds the longitudinal strain rate. The dynamical mass flux seems to be dominated by horizontal divergence of ice flux. These results for elevation changes and strain can be used for verification of ice sheet models (e.g. Colgan et al. 2015; Bondzio et al. 2016, 2017), for determination of ice viscosity, which follows Glen's flow law, and also for validation of satellite measuring methods.

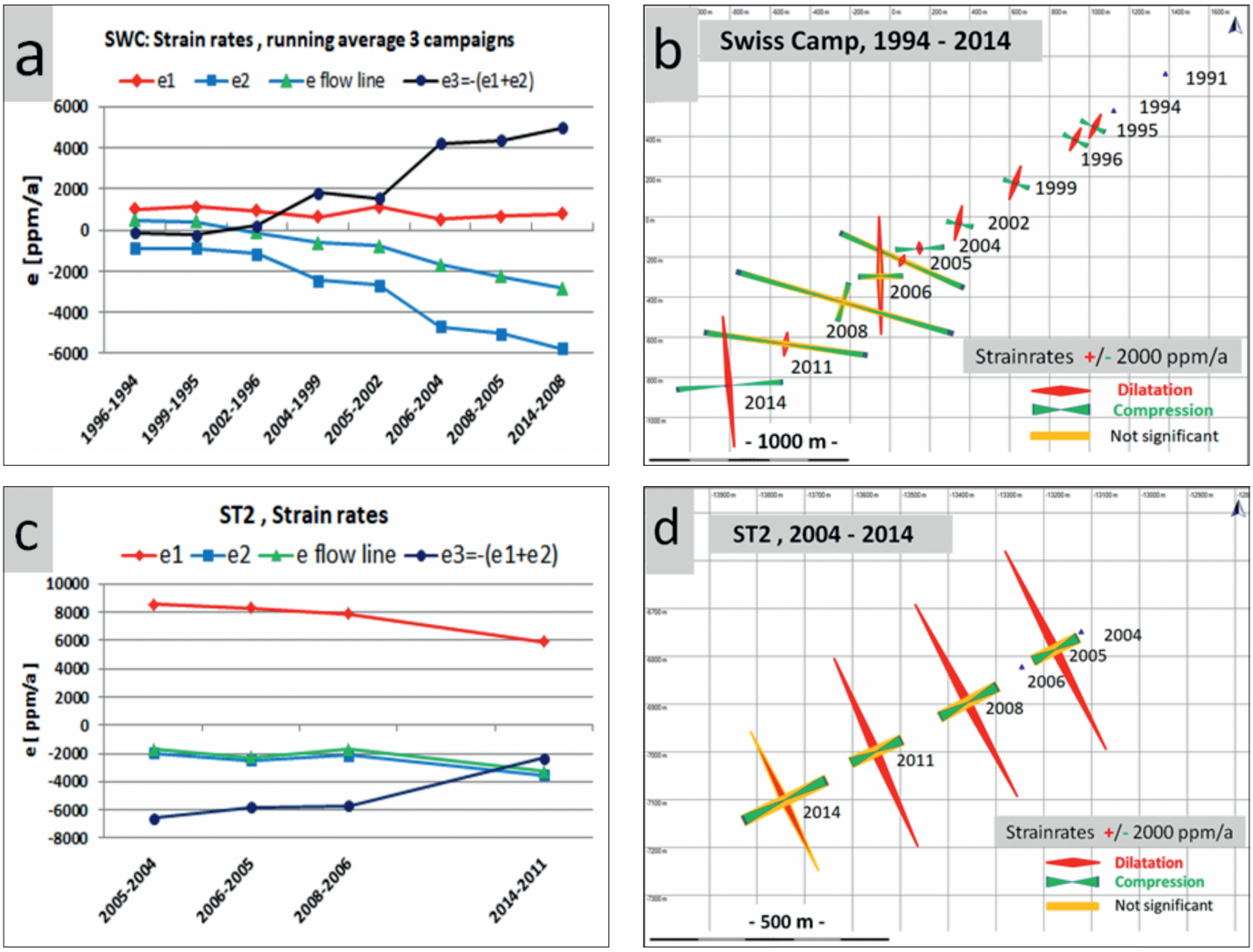

Fig. 11: Strain rates at Swiss Camp: Principal strain e_1, e_2 and in flow line, vertical component e_3 (a). The values in Table 1 are smoothed by a running average over 3 values. The right part (b) shows the principal strain axes between all successive measurements along the moving stake network. The years indicate the end-period (e.g. 2014 = positions 2014–positions 2011). Values with an orange overlay indicate less significance (compare Table 1). Strain rates at ST2: Left part (c): Principal strain e_1, e_2 and in flow line, vertical component e_3. Right part (d): Principal strain e_1, e_2 with principal strain axes between successive measurements along the moving stake network (right). The years indicate the end-period.

Abb. 11: Strainraten bei Swiss Camp: Hauptverzerrungsraten e_1, e_2 und in Fließrichtung, sowie die vertikale Komponente e_3 (a). Die Werte aus Tabelle 1 sind geglättet durch ein gleitendes Mittel über 3 Werte. Der rechte Teil (b) zeigt die Achsen der Hauptverzerrungsrichtungen zwischen allen aufeinander folgenden Messungen entlang des wandernden Pegelnetzes. Die Jahreszahlen geben jeweils das letzte Messjahr an (z.B. 2014 = Positionen 2014-2011). Die Werte mit oranger Überlagerung bedeuten geringere Signifikanz (vgl. Tabelle 1). Strainraten bei ST2: Hauptverzerrungsraten e_1, e_2 und in Fließrichtung, sowie die vertikale Komponente e_3 (c). Der rechte Teil (d) zeigt die Achsen der Hauptverzerrungsrichtungen zwischen allen aufeinander folgenden Messungen entlang des wandernden Pegelnetzes.

ST2	e1	e2	Azimuth e1	e-flow-line 266.4 gon	σ e1,2	t1= e1/σe	t2= e2/σe	e3= = -(e1+e2)	dHe
Campaign	(ppm/a)	(ppm/a)	(gon)	(ppm/a)	(ppm/a)			(ppm/a)	(m/a)
2005-2004	8539	-1949	170,279	-1704	720	***11,87***	-2,71	-6590	***-3,93***
2006-2005	8317	-2514	169,806	-2284	871	***9,52***	-2,88	-5803	***-3,46***
2008-2006	7862	-2142	173,713	-1717	1040	***7,58***	-2,07	-5720	***-3,41***
2014-2011	5911	-3550	171,288	-3281	2159	2,74	-1,64	-2361	-1,41
2008-2004	8202	-2199	171,815	-1874	917	***8,95***	-2,4	-6003	***-3,58***

Tab. 2: Strain rates with standard deviations at ST2. Significance (bold) from t > 3.

Tab. 2: Strainraten mit Standardabweichungen bei ST2. Signifikanz (fett) ab t > 3.

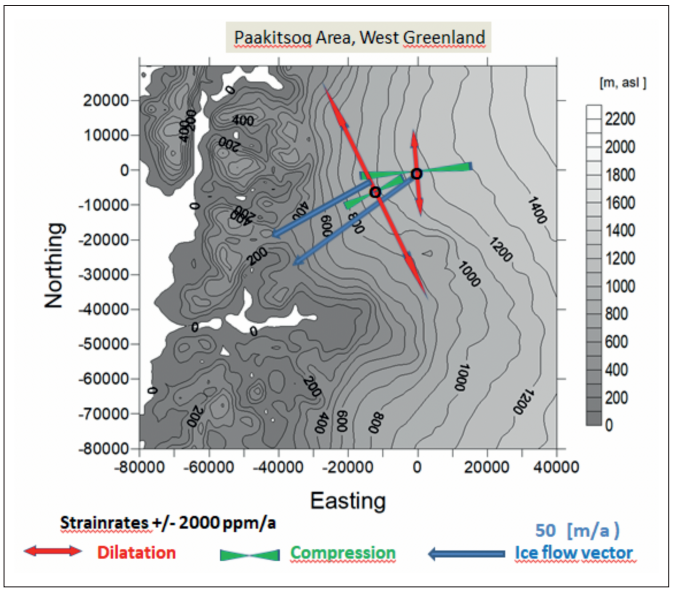

Fig. 12: Ice flow vectors, horizontal strain rates at the survey areas Swiss Camp and ST2, and topography in the Paakitsoq area. The graph shows the results 2011–2014. In flow direction dominates compression, perpendicular stretching. The ice flow azimuth follows the line of the main downhill gradient of the terrain. The locations of SWC and ST2 are in the vicinity of the Jakobshavn Isbrae drainage area.

Abb. 12: Eisflussvektoren und horizontale Strainraten bei den Messgebieten Swiss Camp und ST2 mit der Topographie im Paaqitsoq Gebiet. Die Graphik zeigt die Ergebnisse 2011-2014. In Fließrichtung herrscht Kompression vor, rechtwinklig dazu Ausdehnung. Das Azimut entspricht weitgehend dem Gradienten der Geländeneigung. SWC und ST2 befinden sich im Bereich des Jakobshavn Isbrae Einzugsgebiets.

4. DISCUSSION

4.1 Elevation changes and comparisons with meteorological data

The meteorological data at our study sites are available on the GC-Net (Greenland Climate Network). The Greenland Climate Network (GC-Net) consists of 18 Automatic Weather Stations (AWS) spread throughout Greenland. It is managed by the Steffen group (University of Colorado at Boulder/USA), (Steffen et al. 1996; Box & Steffen 2000; Steffen et al. 2001). The AWS at Swiss Camp and JAR1 (close to ST2) are relevant for our measuring areas.

SWC and ST2 are characterized by different climatic conditions. They are best distinguished by the average monthly temperatures as shown in Fig. 13 (top left), summer air temperature development (top right), net radiation (bottom left), and by the summer albedo (bottom right). The temperature at SWC is significantly lower than at ST2 due to the 170 m higher altitude. The linear trend of the summer temperatures has increased with the years, and both areas are characterized by an offset of about 1.8 K, which shows the colder climate at the higher-situated SWC. Net radiation is typified by high values in July, evidently more extensive at ST2. Here the surface is wetter with less albedo. As a consequence, incoming radiation is absorbed to a greater degree.

The comparison of the elevation changes (dH) with distinct meteorological parameters was first performed with the cumulative dH and the cumulative pdd values. Contrary to what common sense may dictate, in this study pdd was calculated from GC-Net as the sum of hourly, rather than daily, positive air temperature values. So as to compare with the usual definition of pdd (positive degree days), the values should be divided by 24 (hours per day), and 365 (days in a year) for mean annual values. They are shown for both study sites in Fig. 14. There is an almost linear increase of pdd during the measuring periods, in contrast to the accelerated negative elevation changes. The correlation coefficients between (cumulative) dH and pdd are r = -0.93 (SWC) and r = -0.99 (ST2) respectively. While the pdd can be seen to increase almost linearly, the long-term development elevation decrease has accelerated markedly, especially in the more recent, warm years. The smoothed trend line of elevation change clearly shows enhanced melting over the years.

A more detailed insight is demonstrated with elevation changes per year between successive campaigns and the corresponding meteorological parameters (Figs. 15, 16). The correlation coefficients with the summer air temperature are r= -0.13 (SWC) and r = -0.41 (ST2), (Fig. 15a, b). The correlations with pdd here are r = -0.48 (SWC) and -0.18 (ST2) (Fig. 15c, d), that is, much less than with cumulative values. Summer is defined as the average from June, July and August.

At Swiss Camp the temperature record shows a clear warming trend that began around 1995. The distinct increase in the summer air temperatures between 1991 and 2014 (the months of June, July and August) by +0.09 K/a corresponds to the cumulated ice height decrease of 14.41 m over the same time period (until 2014) (Fig. 14), which in turn corresponds with the cumulative mass balance of -13.0 metre water equivalent in the last 23 years. Here the consequence of climate change is clearly visible.

In the first period (1991–2002), the elevation decreased by only -0.25 m/a. It was already enhanced in the middle period (2006–2011) by -0.6 m/a, and even more accelerated in the latest period (2011–2014) by -1.5 m/a (Fig. 15a). This is six times greater than the average in former years. The extremely large elevation changes from 2002 to 2004 coincide with the highest summer air temperatures. Between the campaigns 2006–2008, there is an extreme elevation decrease of -1.04 m per year and, for the period 2008–2011, a very similar decrease of -1.14 m/a is evident. These coincide with higher air temperatures. The correlation is -0.30 and demonstrates the poor dependency. The negative sign is consistent with the positive temperature trend and the negative elevation trend. The decreased elevations agree well with the enhanced melting at the surface, which is also clearly visible from the wide extension of the melt areas on the Greenland ice sheet (Mernild et al. 2011) and extreme melt years, e.g. in 2012 (Nghiem et al. 2012).

At ST2 the results for summer air temperatures averaged between successive campaigns are shown in Fig. 15b. Since 2006 an accelerated elevation decrease of currently -1.65 m/a can be observed at the 170 metre lower-situated area of ST2. This is caused by 1.8 K warmer summer temperatures at ST2 (Source GC-Net, CIRES Boulder/USA, Fig. 13b) compared to Swiss Camp. The correlation with the air temperature between successive campaigns is r = -0.41, hence better than at SWC,

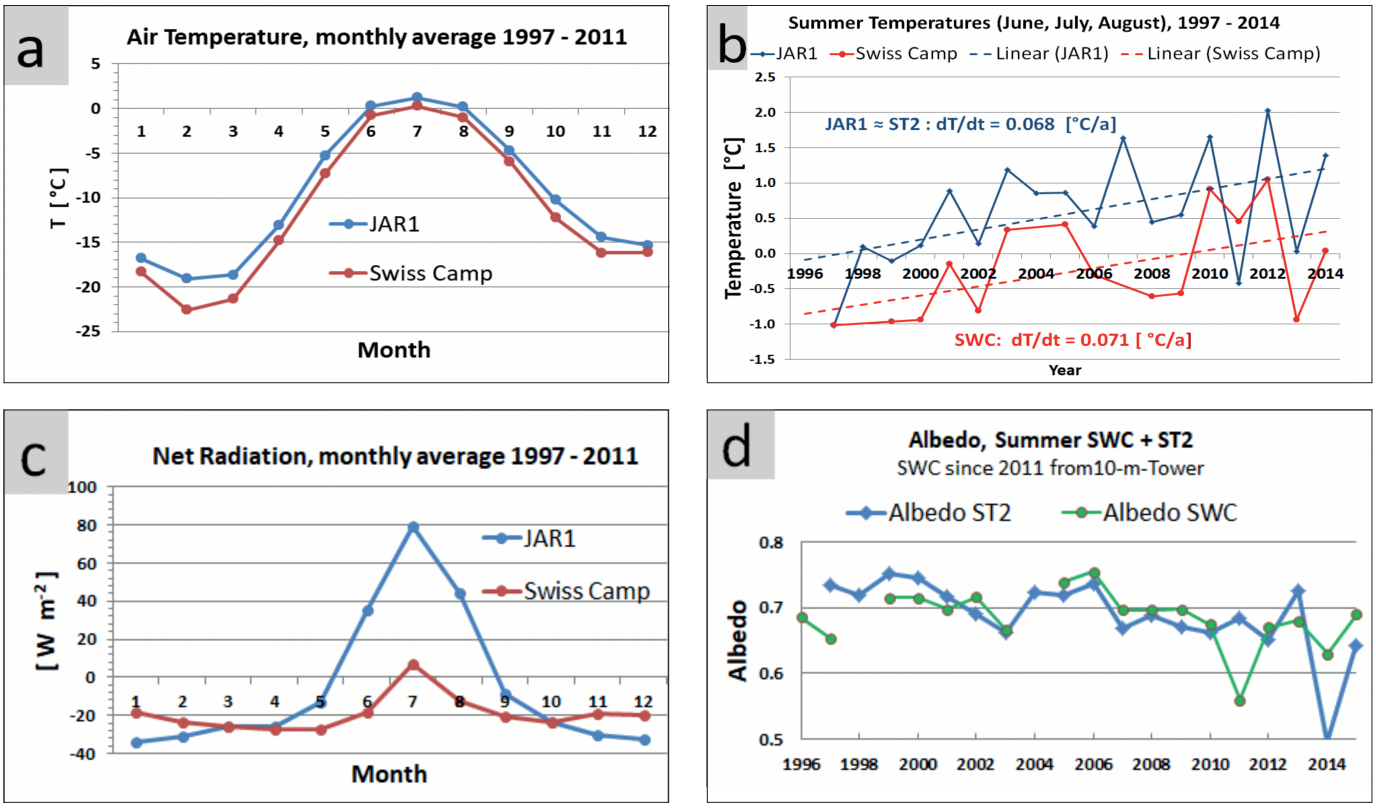

Fig. 13: Climatic condition at SWC and ST2 in comparison (Data from GC-Net). Top left (a): Monthly averaged air temperatures comparing Swiss Camp and of ST2 (corresponding to AWS JAR1). Top right (b): Long-term temperature increase at both stations. Bottom left (c): Monthly averaged net radiation at both stations. Bottom right (d): Summer albedo values (partly adopted from the SWC 10-metre-tower). Clearly visible are the differences between both research areas. Positive degree values are presented in Figs. 14 and 15.

Abb. 13: Klimatische Verhältnisse bei SWC und ST2 im Vergleich (Daten von GC-Net). Oben (a): Monatliche Mittelwerte der Lufttemperaturen bei Swiss Camp und ST2 (Daten von naheliegender AWS JAR1). Oben rechts(b): Langzeitlicher Anstieg der Sommertemperaturen an beiden Stationen. Unten links (c): Monatliche Mittelwerte der Nettostrahlung an beiden Stationen. Unten rechts (d): Sommerliche Albedowerte (tlw. vom SWC 10-Meter-Turm). Klar erkennbar sind die Unterschiede an beiden Messgebiete. Die pdd-Werte sind in den Bildern 14 und 14 enthalten.

however the correlation is worse with pdd (r = -0.18) (Fig. 15b, d). This confirms the dependency on climate change. The relation between ablation and mean temperatures is not linear. Moreover, the relation between positive degree-days and mean temperature is non-linear (BRAITHWAITE 1994,1995).

The study was continued by comparing annual elevation changes and other distinct meteorological parameters. Here we present some examples. Large annual negative net radiation (Fig. 16a) between the geodetic campaigns was found in the summers of 1995 and 2006 (-55 and -80 W m^{-2} respectively), coincident with air temperatures above freezing, indicating a strong albedo-feedback mechanism at the ELA. Only weak interdependencies occur in the summer period with the net radiation balance and the elevation changes (Fig. 16). At SWC we obtain a correlation of r = -0.26, and at ST2 r = +0.08. The large positive net radiation flux 2008 and 2011 at ST2 is indicative of the length of the melting season. High net radiation values can either be the result of low albedo values (i.e., 2008–2011, Fig. 16d), reduced cloudiness (increase in insolation), or increase in atmospheric temperatures (increase in long-wave radiation).

The best correlation of elevation change appears with the summer albedo (Fig. 16c, d). We recognize only a small discrepancy between SWC (r = +0.54) and ST2 (r = +0.89).

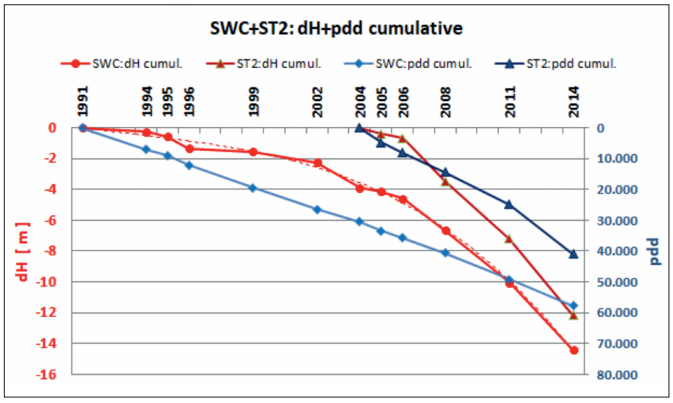

Fig. 14: Comparison of cumulative elevation changes and cumulative pdd across study sites and years. The negative elevation changes (red) are larger at ST2 than at SWC. The pdd values at SWC indicate almost constant values, but at ST2 these have increased since 2011. Here pdd has increased due to warmer summer temperatures.

Abb. 14: Vergleich von kumulierten Höhenänderungen und kumulierten pdd-Werten über Messgebiete und Jahre. Die negative Höhenänderung (rot) ist bei ST2 stärker ausgeprägt als bei SWC. Die pdd-Werte deuten bei SWC auf fast konstante Werte, während sie sich bei ST2 seit 2011 zu wärmeren Sommertemperaturen verstärkt haben.

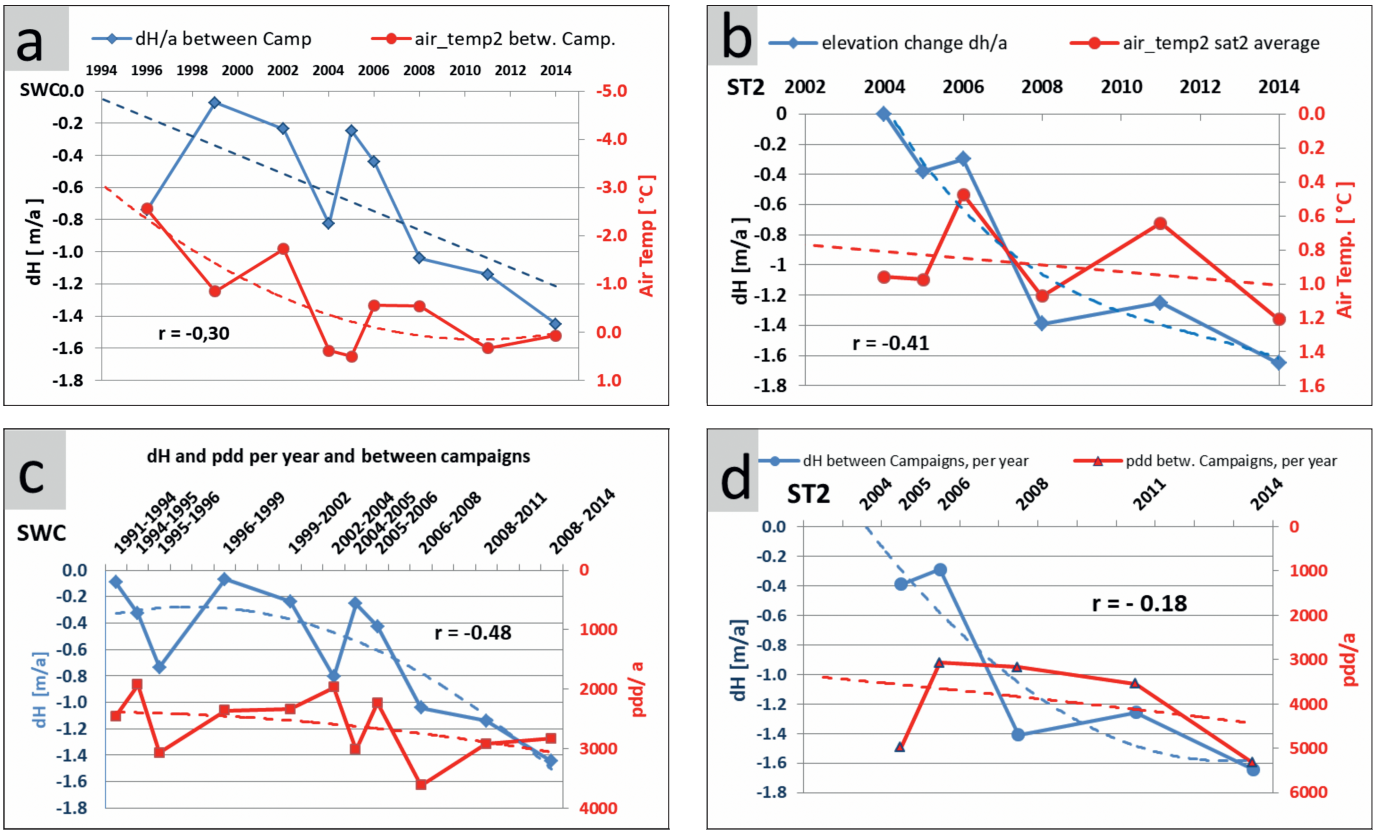

Fig. 15: Comparison of average elevation changes with summer air temperature and pdd per year between successive measuring campaigns at Swiss Camp 1991–2014 (left) and ST2 2004–2014 (right). Temperature data from GC-Net.

Abb. 15: Vergleich von jährlichen Höhenänderungen mit Sommertemperaturen und pdd-Werten zwischen aufeinander folgenden Messkampagnen bei Swiss Camp 1991-2014 (links) und bei ST2 2004-2014 (rechts). Daten von GC-Net.

This is consistent with the generally similar albedo values in the summer period (June, July, August) and the tendentially similar height change in both areas. The number (n) of correlation data pairs is small and varies between 11 and 5. The significance of a correlation coefficient is given by the t-test

$$t = r/\sqrt{(1-r^2)} * \sqrt{n-2} \qquad (4.1)$$

with f = n-2 degree of freedom, so f = 9 to 3.

For r = 0.9 and f = 9 the significance level S = 95 % is t_{95} = 2.262 (resp. S = 99 %, t_{99} = 3.250). With application (4.1) we obtain t = 5,463 > t_{95} = 2.262, so r = 0.9 is significant on the 95 % level (and on the 99 % level respectively). Never significant are correlations around r = 0.4 and less. It must be emphasized that although most correlations are not significant, they are nevertheless indicative of the trends. Substantial correlations with other parameters could not be verified. In the case of this investigation, the fact that the geodetic measurements were not performed every year was found to be unfavourable, while meteorological data were analysed annually.

However, both areas are (now) situated in the ablation area. The ELA, formerly near SWC (1100 m), is now situated at an essentially higher altitude, and has moved tens of kilometres inland (Steffen et al. 2011). An empirical equation gives an ELA of 1418 m at the latitude of the Swiss Camp (Zwally 2002). This statement is confirmed by our snow layer measurements at the stakes. Even at SWC, after 2005 all the snow had melted away in the summer period (compare the data published in Machguth et al. 2016).

At ELA, there is a balance between mass gain from net snow accumulation and mass loss from ablation almost entirely from meltwater runoff. At the time of the 2014 survey, the ice sheet had thinned by more than 1 %, where the ice thickness was approximately 1200 m. The rate of thinning appears to be increasing over time (Fig. 4). The thinning promotes a melt-elevation feedback. Accelerating ice sheet thinning due to surface mass balance is an anticipated consequence of the melt-elevation feedback, whereby decreasing elevation results in increasing melt at any given ice sheet location. The atmosphere has more internal heat, and more downward infrared radiation, as distance from the top of the atmosphere toward sea level increases (Businger & Fleagle 1980). Additionally, lower in the atmosphere, more precipitation falls as rain instead of snow. Ice sheet thinning thus brings the surface down into warmer and wetter parts of the atmosphere, amplifying the enhanced melt and increased rainfall fraction resulting from climate change (Doyle et al. 2015).

4.2 Geodetic mass balance in comparison to measured SMB

In order to derive mass changes from elevation changes it is necessary to correct with the density of ice. We used ϱ = 0.90 g/cm³ (Li & Zwally 2011), other authors, e.g. Weber 2005, mention ϱ = 0.92 g/cm³. The elevation change [m] multiplied

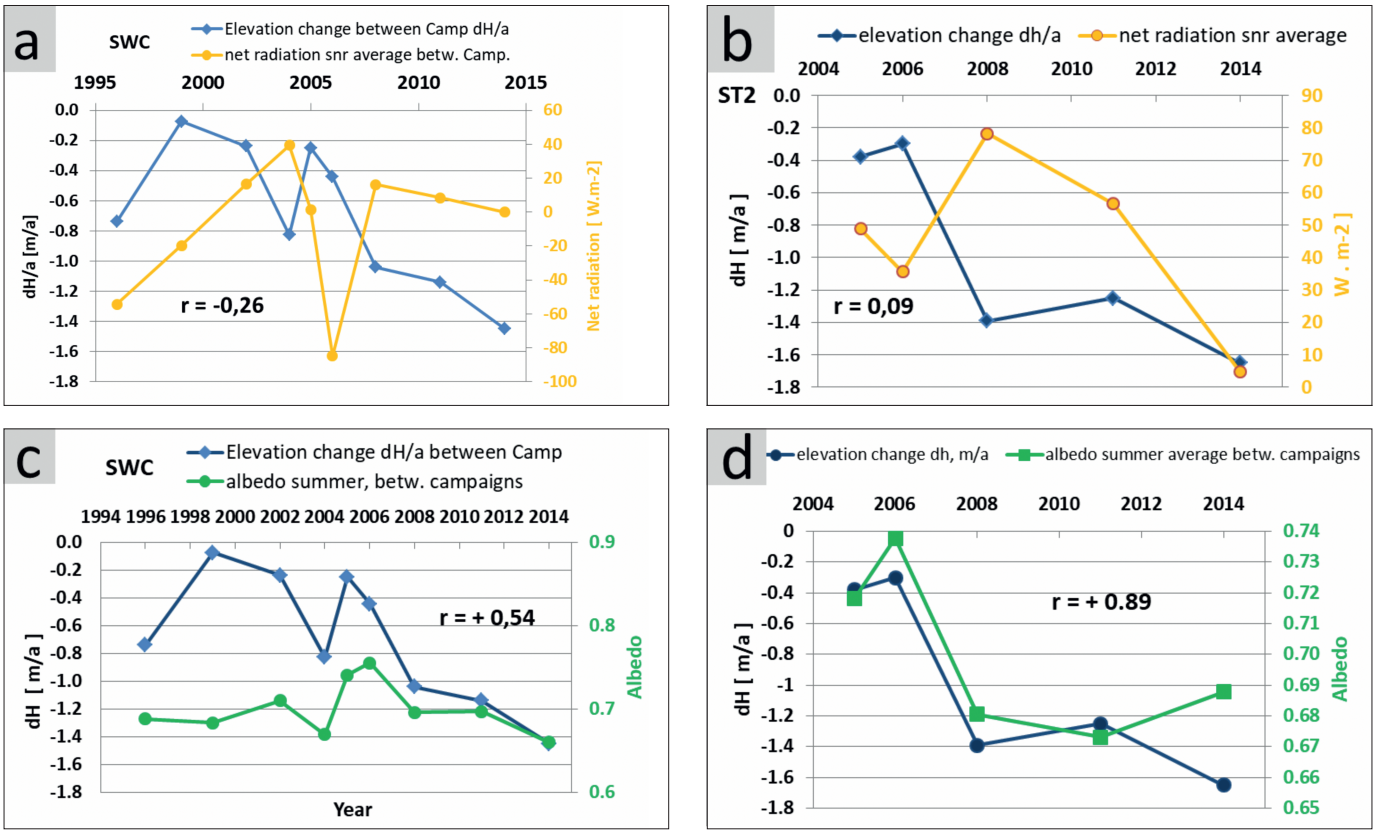

Fig. 16: Correlation between annual elevation changes, net radiation and albedo (SWC left, ST2 right).

Abb. 16: Korrelation zwischen jährlicher Höhenänderung mit Nettostrahlung und Albedo (SWC links, ST2 rechts).

by ϱ gives the corresponding mass change as equivalent to water mass with ϱ = 1 [m, w.e.]. The result from geodetically determined elevation changes per year (dH/a) with reduction for ice density is now called Geodetic Mass Balance (GMB).

The Specific Surface Mass balance (Surface Mass Balance, SMB) is determined by reading the free lengths above the current surface at the stakes, measured in each campaign, the data being published in Machguth et al. 2016. Most of our campaigns were performed at the end of July/the beginning of August, hence with the same meteorological conditions. Also, these height changes are reduced to mass changes by the density ϱ = 0.90 g/cm³ (if ice). If a snow cover was left we used ϱ = 0,55 g/cm³ (Li & Zwally 2011), considering a high part of humidity. Other authors (e.g. Fausto et al. 2018) determine the density for firn in 10 cm depth as 0.315 g/cm³. These SMB values are based on only few stakes (a maximum of 4 in each campaign), however all four stakes were not always useable. At ST2 all stakes had melted out in the years after 2006. Here, estimates (minimum values) were used instead of real measurements, derived from the length in ice at the last visit. Due to the sparse data the standard deviation of SMB is limited to ±0.25 m.

The geodetic mass balance (GMB) was then compared with the specific mass balance from the stakes (SMB). While GPS represents the total mass balance containing both dynamical and meteorological components, the stake measurements give the specific surface mass balance at a few specific points. The difference between GMB and SMB can be interpreted as the dynamic component.

Fig. 17, left, shows that at SWC (SMB for 2006–2008 adopted from Steffen 2011), in almost every year the geodetic mass balance is more negative than the specific mass balance. Both mass balances have the tendency to become more negative over time. Fig. 17, right, shows the geodetic (GMB) and specific surface mass balance (SMB) at ST2 in comparison. The elevation change in the period 2011–2014 in average is -1.65 m/a. The corresponding mass balance is -1.485 m/a w.e. In 2004–2005 and 2005–2006 a large difference between both types of mass balance can be recognized. In later years, both mass changes are almost equal (assuming the minimum SMB estimates after 2006 are correct). This indicates no dynamical thinning or growing – in contrast to the results by the strain analysis (3.4).

Fig. 18 demonstrates the differences between the cumulated geodetic and surface mass balances. At SWC we recognize a systematically growing difference between both curves. The accuracy for GMB at the final year 2014 can be assessed by error propagation to ±0.2 m, for SMB to ±1 m. These discrepancies are probably caused by dynamics and they are an important result for ice sheet modelling at this location. It is arguable that the mass loss derived by the geodetic method is greater than can be explained by SMB alone. This is a clear indication of dynamic thinning, which is shown to increase over the years, particularly after 2002. The dynamic part as difference between GMB and SMB (stakes) cumulate to

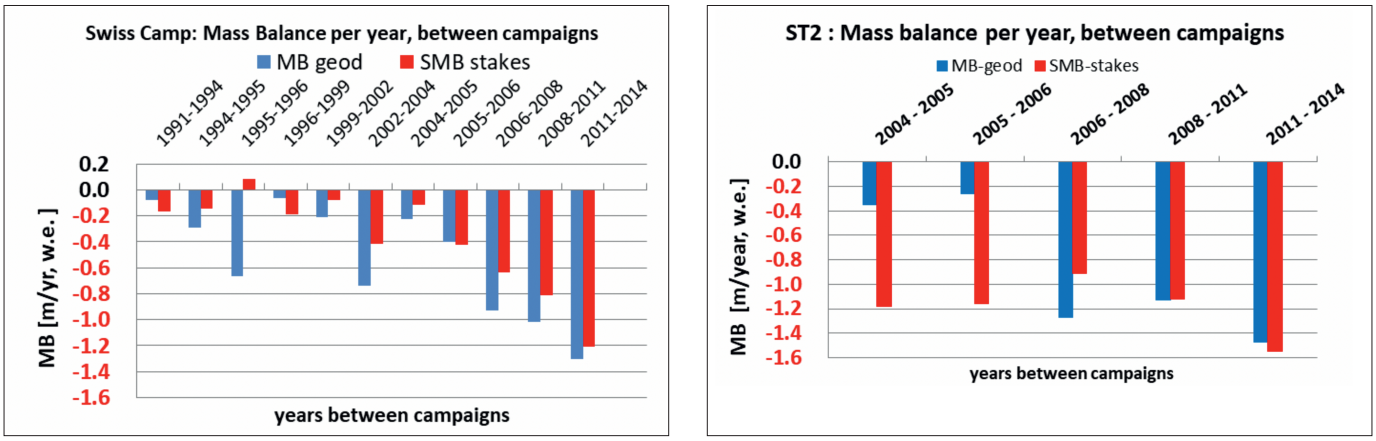

Fig. 17: Geodetic Mass Balance (GMB) and Specific Surface Mass Balance (SMB) per year between measuring campaigns at Swiss Camp 1991–2014 (left) and ST2 (right). Note that at ST2 the SMB after 2006 are (minimum) estimates.

Abb. 17: Geodätische Massenbilanz (GMB) und Spezifische Oberflächenmassenbilanz (SMB) pro Jahr zwischen den Messkampagnen bei Swiss Camp 1991-2014 (links) und bei ST2 (rechts). Zu beachten ist, dass es sich bei ST2 ab 2006 nur um Schätzwerte (Minimalwerte) handelt.

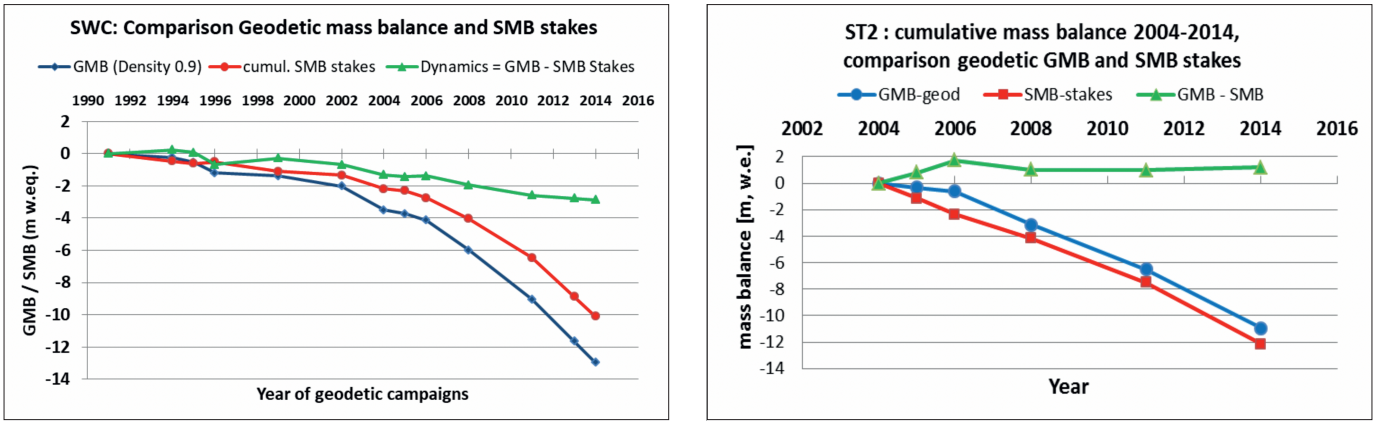

Fig. 18: Comparison of cumulative Geodetic Mass Balance (GMB, blue), Specific Surface Mass Balance (SMB, red) from stakes, and dynamic residual (green), at Swiss Camp 1991–2014 (left) and at ST2, 2004–2014 (right). The dynamical residual (GMB – SMB) at SWC is ca. -2.3 m, or 18 % of the total mass change in 2014.

Abb. 18: Vergleich von kumulierter Geodätischer Massenbilanz (GMB, blau), Spezifischer Massenbilanz (SMB, rot) aus Pegelablesungen und dynamischer Anteil (grün), bei Swiss Camp 1991-2014 (links) und bei ST2, 2004-2014 (rechts). Der dynamische Anteil (Differenz GMB – SMB) beträgt 2014 bei SWC ca. -2.3 m oder 18 % der totalen Massenänderung.

-2.34±1 m w.e. or 18 % of the total mass change in 2014. As an explanation we can suggest several possibilities:

- Now the ice flows faster out of the SWC area than according to an equilibrium.
- The ice flows slower into the SWC area than according to an equilibrium.
- Both: the ice flows faster out of and flows slower into the SWC area.
- Precision of SMB measurements due to limited number of available stakes.

The discussion of the ice flow velocity and the strain analysis in Section 4.3 below will provide more information. At ST2 the mass balances GMB and SMB-stakes show the opposite behaviour compared with Swiss Camp. The annual results 2004–2005–2006 (Fig. 17, right) and the cumulative mass balances (Fig. 18) indicate more negative SMB-stakes values than GMB. Therefore, the dynamical part in GMB is positive here.

4.3 Velocity and deformation in the context of dynamic feedback

The ice flow velocities at Swiss Camp and ST2 behave contrarily. At SWC the annual mean flow velocity is 0.32 m/d, while at ST2 the ice moves slower at 0.19 m/d (Fig. 9). At SWC the velocity increases over time. At ST2 it decreases over time. Principally it is possible that the flow velocity is dependent on the location. The acceleration at SWC might be caused by the displaced stake network due to the ice movement. In one year, the stakes move downhill about 115 metres, thus from 1991 to 2014 the stake network was displaced by about 2.7 km. In order to check this influence, we used the configuration of stakes 106 and 121, which are almost aligned in the same flow line. As can be seen in Fig. 2, left, the stake 121-2004 had nearly moved to the same location as 106-1994, or stake 121-2008 had moved to 106-1999. Comparable positions are: (1) stake 106-1999/2002, v = 0.316 m/d with stake 121-2008/2011, v = 0.330 m/d, and (2) stake 106-1994/1995, v = 0.309 m/d with stake 121-2004/2005, v = 0.318 m/d. After ca. 10 years the velocity had increased

by 0.009 m/d and 0.014 m/d respectively, which proves the flow acceleration at the same location. The older velocities are significantly slower compared with those in later years.

At ST2 the flow velocity is slower than at SWC and decreases over time. This is remarkable, because melt water should be produced at an increasing rate at the lower altitude of ST2. A significant number of moulins rapidly drain the surface melt water down to the bedrock. Further, the warmer atmosphere at the lower altitude should facilitate melt water production and basal sliding all the more. However, the relationships between surface velocity and meltwater input continue to be unclear (Morriss et al. 2013). In our case, the velocity decrease of the moving stake network is probably caused by the ascending bedrock topography near the coastal mountains. A similar comparison of velocities at the very same position (as at SWC) is unfortunately not possible at ST2.

In Fig. 11 we demonstrated that the ice flow velocity in summer is significantly faster than the annual average. Both research areas show here a similar acceleration during summer, probably forced by rapid variations in meltwater input to the subglacial drainage system from the ice sheet surface. For a long time (Zwally et al. 2002; Bartholomew et al. 2012) it has been assumed that increased melt water as a result of higher summer temperatures causes faster basal sliding at the bedrock. This theory is confirmed by recent investigations (Catania et al. 2008; Price 2008; Colgan et al. 2011a, b, c and 2012; McGrath et al. 2011).

The most important information relates to the elevation and mass change respectively. In an equilibrium state they should not change. Increasing and decreasing masses should hold an equilibrium. The total mass balance consists of the surface mass balance (SMB) and of the dynamical components by influx and outflux from higher to lower regions. The geodetic measurements of the surface heights and their temporal changes contain the summarising effect of both of these components (constant density assumed) and indicate whether the equilibrium is still valid.

The longitudinal strain between SWC and ST2 show a contraction of the distances increasing permanently and at an accelerated rate. This is explainable by the different global flow behaviour of both areas. While at SWC the ice flows faster and at an accelerated rate, at ST2 it flows slower and at a decelerated rate. This velocity difference (SWC: 0.324 m/d or 118.2 m/a, ST2: 0.193 m/d or 70.4 m/a) results in a shortening of 47.8 m/a. The longitudinal strain generates a compression that leads to dynamical mass growth in the marginal ice sheet region SWC-ST2. Here the influence of the bedrock topography becomes apparent. While at SWC the ice flows into a kind of trough, at ST2 it flows against the ascending marginal mountains. SWC and ST2 are situated in the catchment area of the Jakobshavn Isbrae. Recent ice flow models can incorporate the variability in basal topography and can produce realistic flow fields (Bondzio et al. 2016, 2017).

Our results follow from a long-term analysis. Short-time seasonal strain rates in the period 2006–2007 are published by Rumrill (2009). Her data are also discussed in Hoffmann et al. 2011, where a connection between hydrology (melt and subsurface drainage) is considered. An interpretation of longitudinal strain within the stake networks is possible if the strain component perpendicular to the ice flow is zero (Paterson 1994). Yet, contrarily, the results in our research areas from the strain analysis show distortions in all horizontal directions (e_1, e_2). The main flow azimuth is superimposed by differential movements in other directions across the area.

According to the results in Table 1, the dynamical component (dM_e) calculated from the vertical strain e_3 is now shown in Fig. 19 for a balance year and for significant strain values only. dMe should agree with the difference GMB – SMB (stakes). We have to conclude that, although agreement can be fairly well established in the initial years, since 2004 no agreement can be ascertained and even the sign is contrary.The causes for this disagreement could be: (1) The condition of homogeneity in the moving stake networks is not fulfilled, and (2) dislocation of the networks between two campaigns.

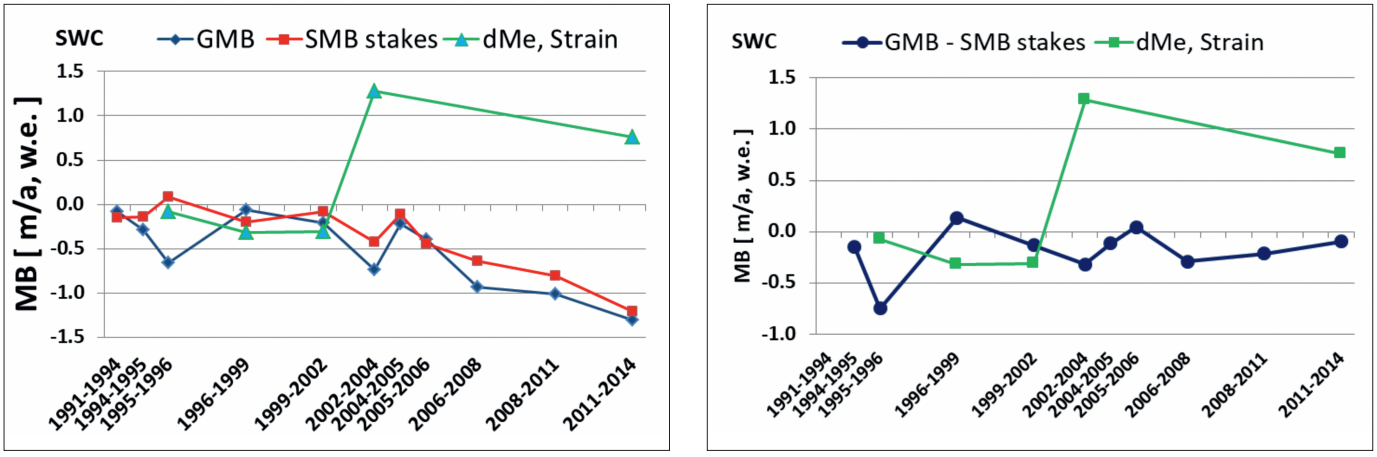

Fig. 19: (Left) Comparison of the dynamical part (dM_e) of mass balance from vertical strain (green) with Geodetic Mass Balance GMB (per year) and SMB (stakes). Only significant strain results are used for Swiss Camp 1991–2014. (Right) Difference Geodetic Mass Balance GMB minus SMB stakes compared to dM_e from vertical strain rate e_3. Values for metre w.e. per year.

Abb. 19: (Links) Vergleich des dynamischen Anteils (dM_e) der Massen Bilanz berechnet aus der vertikalen Strainrate (grün) mit Geodätischer Massenbilanz GMB (pro r) und SMB (Pegel). Hierbei wurden für Swiss Camp 1991–2014 nur signifikante Strainwerte verwendet. (Rechts) Differenz Geodätische Massenbilanz minus SMB (Pegel) verglichen mit dM_e aus vertikaler Strainrate e_3. Werte in Meter w.e. pro Jahr.

SWC: Strain rates all triangle combinations, 1994–2004			
ranges (5 values)	**AZ e1 [gon]**	**e1 [ppm/a]**	**e2 [ppm/a]**
Average	0.9 -20.3	309 - 2090	708 - 1842
Std-Dev of Av.	4.4 -11.8	8 - 689	20 - 912
Std-Dev in %.		1 - 85 %	2 - 82 %

Tab. 3: Principal strain rates calculated from all 4 triangles for Swiss Camp.

Tab. 3: Hauptverzerrungsraten für alle 4 Dreiecke im Gebiet Swiss Camp.

ST2: Strain rates all triangle combinations, 2004–2006			
ranges (3 values)	**AZ e1 [gon]**	**e1 [ppm/a]**	**e2 [ppm/a]**
Average	369.2 - 370.0	8379 - 8517	2009 - 2591
Std-Dev of Av.	2.44 - 2.77	842 - 972	317 - 489
Std-Dev in %.		10 - 12 %	16 - 19 %

Tab. 4: Principal strain rates calculated from all 4 triangles for ST2.

Tab. 4: Hauptverzerrungsraten berechnet aus allen 4 Dreiecken bei ST2.

The strain calculation from the distortion of an area (represented by a stake network) is only correct if the ice surface is deformed homogeneously. In order to check the homogeneity, we investigated the standard deviation ($\sigma\ e_{1,2}$) of the strain rates after the adjustment. Tables 1, 2 contain these values, but they do not show significance in all cases or all years. Even with significant strain rates the $\sigma\ e_{1,2}$ is relatively large to the order of 3800 ±531 ppm/a (e.g. SWC 2011–2014), which means a distortion of 5.7±0.8 m/a for a 1.5 km extension of the network. This is obviously more than the measuring accuracy (ca. 5-10 cm) and points to other irregularities, such as inhomogeneous ice flow vectors due to topographical forcing on the surface and/or in the bedrock. The homogeneity condition is satisfied only weakly.

Principally it is possible to derive the strain rates in every single stake triangle without a least-squares adjustment. This would also allow for a comparison that provides insight into the homogeneity. Although at Swiss Camp the triangles are geometrically designed too slim, this calculation was performed over a number of years (1994–2004) with the results presented in Table 3 below. At ST2 the net design is very regular and more suitable for a homogeneity test within triangles. Examples are shown for the campaigns 2004–2005–2006 (Table 4).

Tables 3 and 4 list the ranges of the average values for azimuth, e_1 and e_2 with their variations between the 4 possible triangles calculated in all combinations. At SWC (Table 3) we recognize a large span within one strain calculation. The standard deviations vary substantially, for the azimuth up to ±12 gon, and for e_1 and e_2 up to 85 and 82 % respectively. Here the homogeneity in strain is poor, but this is partly caused by the worse triangle configuration. The same results at ST2 (Table 4) demonstrate much better homogeneity. The standard deviations from the varying values are much better with ± 2.5 gon in azimuth, 12 % for e_1 and 19 % for e_2. Here the homogeneous strain parameters can be confirmed.

The detailed calculations in all triangle combinations with the results in Tables 3 and 4 were executed for the years limited until 2004 or 2006 (SWC and ST2 respectively). For these years it was possible to compare them with the significance test ($t = e_{1,2}/\sigma_e$) of e_1 and e_2 in relation to the adjusted values in the over-determined case (ABCD). In most cases we find a coincidence between t and the standard deviation of the average from the different triangles. Large values in Tables 3 and 4 coincide with insignificant strain parameters in Tables 1 and 2, and small values coincide with significant strain parameters. Therefore, we can generalize the statement: all strain values in Tables 1 and 2 that are not significant can be declared as inhomogeneous values, and vice versa.

The original idea and assumption for the strain analysis is that the network (representing the area) is only distorted by strain and not shifted during the two campaigns. The cuboid assumed to be deformed under the incompressibility condition should not be displaced. In reality we observed the surface (represented by the shifted stake network) at two different locations. The networks and the horizontal coordinates are displaced by the annual ice flow velocity. The affine transformation eliminates this mean longitudinal dislocation by two of the six transformation parameters. Thus, the strain rates were calculated from two shifted networks with the assumption that the surface is deformed by horizontal, homogenous strain only. In reality, this condition is not fulfilled. We only contemplate horizontal coordinates of a shifted and distorted surface. The distortions are in truth an expression for the differential ice flow vectors of the stake motion in size and azimuth.

The calculation of a vertical component derived by strain using the incompressibility condition is only correct if the ice column is not shifted or, respectively, only shifted along a horizontal surface, a horizontal bedrock and constant ice thickness. In reality, neither the terrain surface is horizontal nor the bedrock underground. The DEM data from DTU (2005) show that at SWC the ice thickness varies from 0 to 20 metres, and the bedrock between 4 and 25 m between consecutive campaigns. Over the whole flow path (ca. 2.4 km in 23 years), the ice thickness was reduced by 120 m, and the bedrock rose by 107 m.

At ST2 the bedrock rises along the flow path represented by the positions of stakes ST200 and St202. The ice thickness here varies by 40 metres to a minimum in the middle of the longitudinal profile (cross section). Therefore, we can expect different conditions for the strain behaviour influenced by the mountains in the rock underground. The area at ST2 is not shaped by a uniform surface topography, which indicates different ice flow vectors and, therefore, locally different strain rates. The interpretation of a strain derived vertical elevation change is therefore limited.

4.4 Satellite-derived results compared to ground measurements

The high quality of the digital terrain models was used for comparison with elevation and elevation change data from satellite altimetry. In fact, the areas are small, ca. 2×2 km^2, meaning that a few footprints of the satellite signals always fell into our areas. Another difficulty lay in the simultaneity of the satellite and ground measurements. Therefore, only spot test samples were possible. Over the years the following ice satellites could be evaluated.

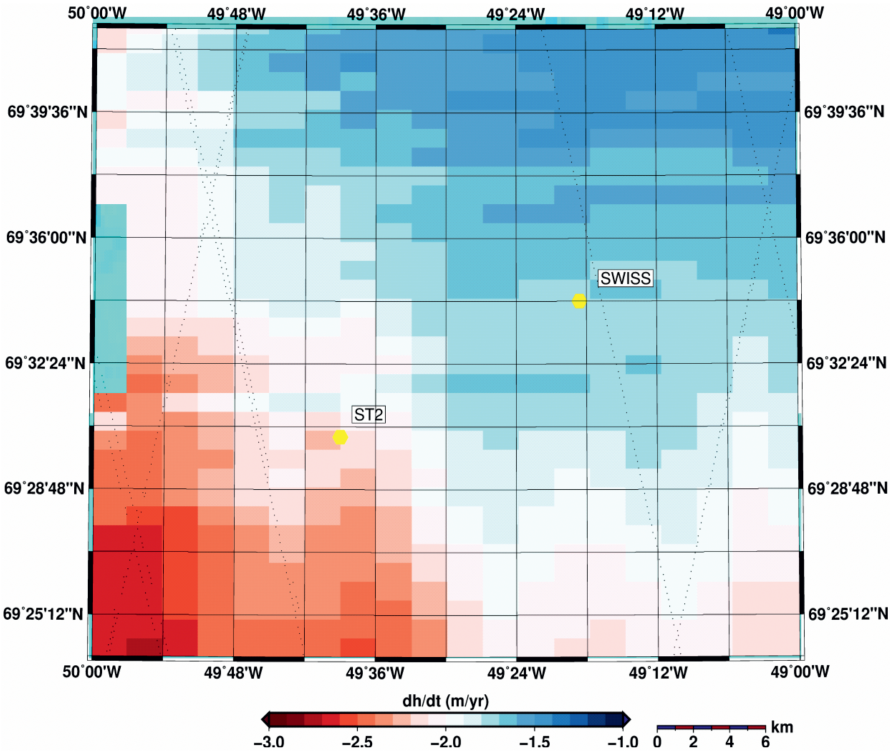

Fig. 20: Elevation change model from CryoSat-2 for 1/2011 to 1/2014 in the regions Swiss Camp and ST2. Source data and image: HELM et al. 2014.

Abb. 20: Höhenänderungsmodell aus CryoSat-2 für den Zeitraum 1/2011 bis 1/2014 in den Regionen Swiss Camp und ST2. Datenquelle und Bild: HELM et al. 2014.

4.4.1 ICESat

ICESat (Ice. Cloud and Land Elevation Satellite) is a US satellite that orbits at a height of 600 km with an inclination of 94°. The measuring device is the Geoscience Laser Altimeter System (GLAS), with 40 impulses per second. Along the flight track the footprints on the earth surface have a distance of 172 m and a diameter of 60 m. The data were available from the homepage of NSIDC (National Snow and Ice Data Center), http://nsidc.org/data/icesat/order.html. ICESat was operable from 2003 to 2009; the launch for its successor, ICESat-2, is scheduled for 15 September 2018. In 2005 we could compare one track with an overflight on 21 May 2005 at Swiss Camp. In order to compare the heights with our digital elevation model some corrections were necessary:

- Ellipsoid conversion: ICESat was referred to the ellipsoid used at TOPEX/Poseidon, our heights are referred to WGS84. Height correction -0.70 m. (http://nsidc.org/data/icesat/faq.html#alt7, Altimetry Products. FAQ Nr. 7).
- Reduction due to a snow layer between different measuring dates from ICESat and GPS (-1.41 m). Data from AWS (GCNet) at Swiss Camp.

Unfortunately, only 5 points in the SWC area were available for the comparison. The height discrepancies (GPS – ICESat) were, on average, -0.13 ± 0.06 m. With regard to the definition of the snow/ice surface this is a very good result.

4.4.2 CryoSat-2

CryoSat-2 is a satellite from the European Space Agency (ESA). It is operable since 2010.
The height measurement device is the SIRAL (Synthetic-Aperture Interferometric Radar Altimeter). Unfortunately, all the level-2-results from ESA were situated outside of our areas and no direct height comparisons were possible.
However, comparisons were possible with published elevation changes. HELM et al. (2014) derived maps of elevation change dh/dt, using three full cycles of ESA level 1b data acquired between January 2011 and January 2014. They present the first elevation change maps of Greenland (and Antarctica) derived from CryoSat-2 data. This is the same time interval as we measured, however, time-shifted (HELM January-January, HFT August-August). HELM presents an elevation change map for all of Greenland. A limited map to the zone of our campaigns is shown in Fig. 20. The general result shows an increased negative elevation change in direction to the catchment of the Jakobshavn Isbrae.

HELM provided us with more detailed digital data of his elevation change model with a grid of 1000 metres. Due to our relatively small areas, only few points (7 at SWC, 6 at ST2) were comparable. The result is summarized in Table 5. The comparison shows on average differences of 0.24 m/a (SWC) and 0.48 m/a (ST2). The relatively large discrepancies could

	Elevation change 2014–2011 [m/a]	
	Swiss Camp	ST2
GPS (Stober)	-1.46 ± 0.02	-1.65 ± 0.04
CryoSat-2 (HELM)	-1.70 ± 0.004	-2.13 ± 0.028
Difference GPS – CryoSat-2	**0.24**	**0.48**

Tab. 5: Elevation changes 2014–2011 from ground measured GPS (STOBER) compared with CryoSat-2 elevation change model (HELM).

Tab. 5: Höhenänderungen 2014-2011 aus GPS Bodenmessungen (STOBER) im Vergleich zu CryoSat-2 Höhenänderungsmodell (HELM).

be caused by the shifted timeframe (CryoSat: January-January and GPS: August-August). Seasonal influences are to be expected, especially at the lower-situated area of ST2 as a result of greater melting rates in summer. In January both areas are still covered with a thick snow layer while, by August, the snow has melted away. The extent to which the radar signal of CryoSat-2 penetrated into the snow layer is not clear, however, which generates a possible inaccuracy. As mentioned above, the HFT-heights are always referred to the ice horizon. Other evaluation errors are also possible. For instance, a small roll angle error leads to a cross-track position error, which at first order does not lead to a height error. But a position error leads to systematic wrong heights compared to the GPS heights in the inclined terrain.

4.4.3 Operation IceBridge

NASA's Operation IceBridge (OIB) is an airborne effort to bridge the altimetry data gap between ICESat and ICESat-2. It employs the Airborne Topographic Mapper (ATM), a scanning laser altimeter that measures changes in ice surface elevation. We compared a data set with elevation changes from the period 2014–2011 in the Swiss Camp and surrounding area (30 km to the West, 10 km East, 30 km South and 10 km North). The data was downloaded from NSIDC and contained Easting, Northing, ellipsoidal height, dh/dt, and RMS-error. The dh/dt values were modelled by SURFER and interpolated for the positions SWC and ST2. Alternatively, we picked out the nearest point. The interpolation error can be large, because the data is distributed rather sparsely. Fig. 21 below demonstrates the flight tracks with available data, where the long data gaps of up to 10 km between each are clearly visible.

The results we obtained are as follows:
OIB interpolated, dh/dt: SWC = -1.6 m/a, ST2 = -1.2 m/a
OIB nearest point, dh/dt: SWC = -1.69 m/a ±0.11 (D = 1.75 km), ST2 = -1.06 m/a ±0.40 (D = 1.82 km)

Compared to our GPS ground measurements for 2014–2011, we obtained:

GPS dh/dt: SWC = -1.45 m/a, ST2 = -1.65 m/a ±0.05 m/a

In order to assess the accuracy of OIB, Fig. 21, right, shows the dependency Height/RMS. The accuracy increases with height. This is caused by stronger influences from terrain inclination in the lower altitudes near the ice margin. SWC and ST2 are situated at altitudes of around 1000 to 1200 m. Here the RMS can be assessed between 0.1 to 2 m, which is approximately ±1 m, on average. As far as these errors are concerned, at SWC the OIB solutions were not too far away from the GPS ground truth values. Particularly at the lower-situated position, ST2, however, the OIB values were found to differ significantly from GPS. In conclusion then, although the use of dh/dt from OIB provides a useful impression for the small-scale general overview of elevation change, it cannot be recommended for detailed studies.

4.4.4 TanDEM-X

TerraSAR-X is a German national remote sensing satellite that has been implemented in a public-private partnership between the German Aerospace Center (DLR) and EADS Astrium GmbH. The TerraSAR-X (TSX) satellite was successfully launched on 15 June 2007. A second identical satellite, TanDEM-X (TDX), followed three years later. The aim of the mission is a digital terrain model of the earth with a resolution of 12 m and a relative height accuracy of 2 m (KRIEGER 2013). As is the case with CryoSat, both satellites work with the interferometric Synthetic Aperture Radar (SAR) mode.

For the campaign 2014 TanDEM-X was scheduled from DLR (in cooperation with Prof. Dr. H. ROTT, University of Innsbruck and Enveo IT GmbH) in such a way that the satellites measured the terrain at Swiss Camp almost simultaneously to

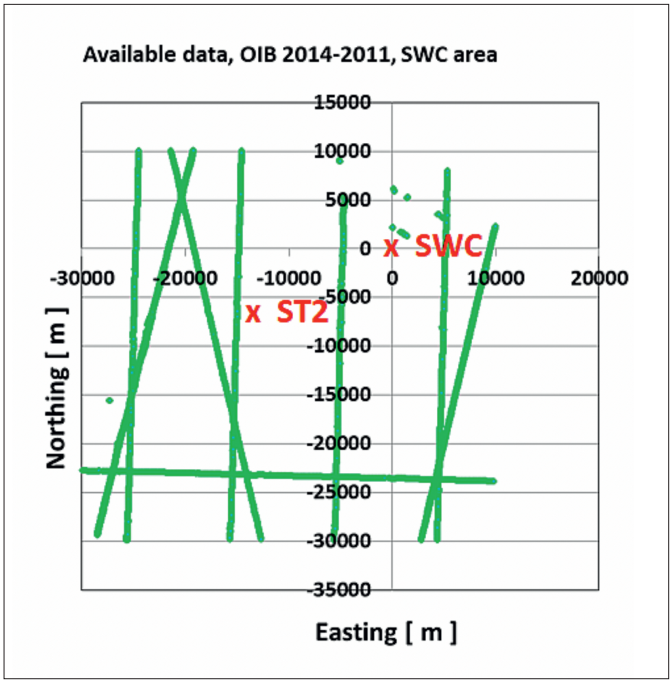

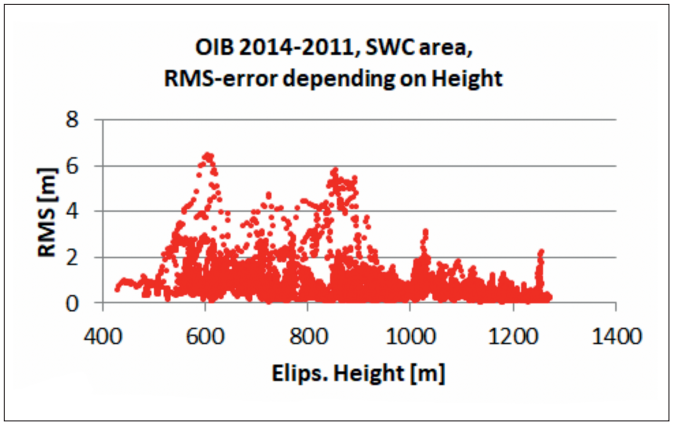

Fig. 21: Data dh/dt from Operation IceBridge, 2014–2011. (Left) Distribution of data at the SWC and ST2 area. This demonstrates the long data gaps between the flight tracks. Local cartesian projection with its origin in SWC 106/1999. (Right) RMS-errors indicated by Operation IceBridge data 2014–2011 and their dependency on ellipsoidal height.

Abb. 21: Daten dh/dt von Operation IceBridge, 2014–2011. (**Links**) Verfügbarkeit der Daten in den Gebieten SWC und ST2. Es zeigt die großen Datenlücken zwischen den Flugbahnen. Lokale kartesische Projektion mit Ursprung in SWC 106/1999. (**Rechts**) RMS-Fehler bei Daten von Operation IceBridge, 2014–2011, und ihre Abhängigkeit von der ellipsoidischen Höhe.

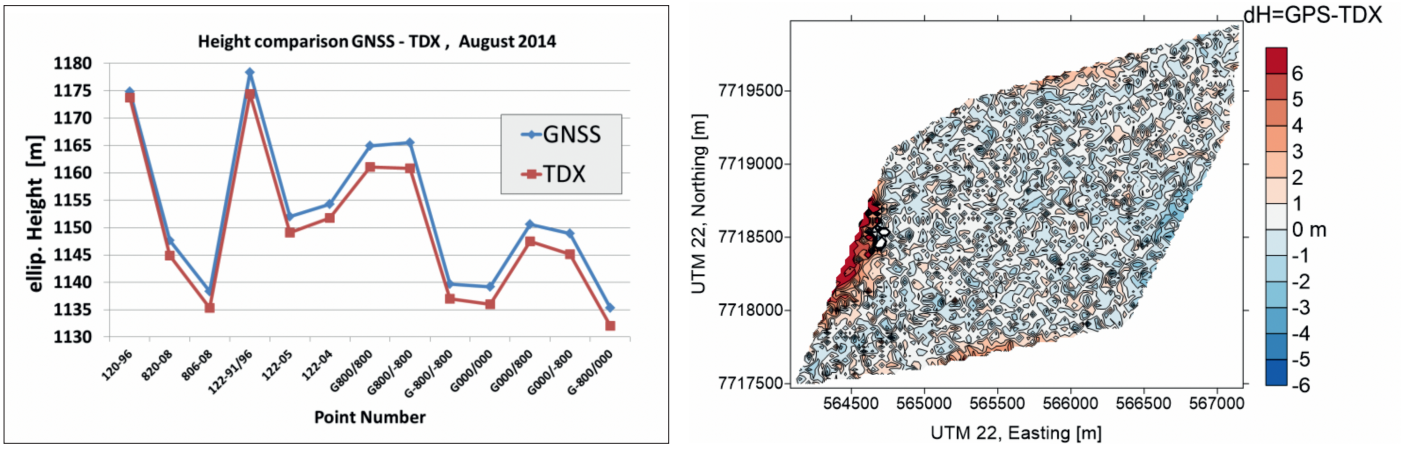

Fig. 22: (Left) Comparison of uncalibrated heights from TanDEM-X and GPS, example with some selected points at SWC. The average height offset from all 1847 points is 3.14 ±0.025 metres. The TDX-heights lay systematically at a lower level. (Right) Height discrepancies between TanDEM-X (16 August 2014) and GPS ground measurement (5 August 2014) after a best fit by an offset of 3.14 m.

Abb. 22: (Links) Vergleich unkalibrierter Höhen aus TanDEM-X mit GPS Bodenmessungen, Beispiel mit einigen ausgewählten Punkten bei SWC. Der durchschnittliche Höhenversatz aller 1847 Geländepunkte ergab 3.14 ±0.025 m. Die TDX-Höhen liegen systematisch tiefer. (Rechts) Restliche Höhenabweichungen zwischen TanDEM-X (16. August 2014) und GPS Bodenmessungen (5. August 2014) nach bestmöglicher Anpassung durch den Versatz von 3.14 m.

our ground measurements. The time shift in August 2016 was only 11 days. DLR (Rott & Floricioiu 2014) provided one (uncalibrated) TanDEM-X DEM (track from 16 August) with a horizontal resolution of 5 m for the Swiss Camp area. The uncalibrated heights (1847 points) differ from the GPS terrain model by an offset of 3.14 ±0.025 m (Fig. 22, left). The standard deviation for one point was 1.07 m. After a calibration by a best fit over the area (1847 points) the residuals resulted mostly between +2m and -2m. The remaining discrepancies between the adjusted TanDEM-X heights and our GPS heights are shown in Fig. 22, right. Some large discrepancies are not realistic and are caused by poor constitution of the digital terrain model at the borders of our field measurements. The achieved accuracy of 1.07 m is very realistic for satellite altimetry by TanDEM-X after local calibration.

4.4.5 Ice flow velocity

Ice movements are usually determined by remote sensing from satellites or with photographic/photogrammetric measurements using feature tracking. Our ground measurements can be used as ground truth for validation as presented by some examples. A current data set for our campaigns is available from Nagler et al. 2015. They applied the offset tracking technique on SAR image pairs of repeat pass orbits to derive surface displacements by the interferometric SAR method. Sentinel-1 IW, TerraSAR-X and ALOS PALSAR (Advanced Landside Observing Satellite, Phased Array type L-band Synthetic Aperture Radar) were applied. ALOS PALSAR is an active microwave sensor using L-band frequency to achieve cloud-free and day-and-night land observation. In our region,

Swiss Camp	69° 33' 34" N	49° 21' 12" W	H = 1170 m	
Method	**Date**	**Velocity [m/d]**	**Azimuth [gon]**	**Source**
PALSAR	22/11/2009 - 5/01/2010	0.264	260.29	NAGLER 2015
Sentinel-1	03/01/2015 - 15/01/2015	0.314	261.84	NAGLER 2015
Sentinel-1A+B, average	Oct 2014 - Sep 2017	0.340		WUITE 2017
GPS	2008 - 2011, interpolated	0.326	260.91	Stober/Wössner
GPS	2011-2014, average	0.327	260.23	Stober/Hönes
ST2	**69° 30' 28" N**	**49° 39' 18" W**	**H = 1000 m**	
PALSAR	22/11/2009 - 5/01/2010	0.174	271.14	NAGLER 2015
Sentinel-1	03/01/2015 - 15/01/2015	0.177	271.61	NAGLER 2015
Sentinel-1A+B, average	Oct 2014 - Sep 2017	0.185		WUITE 2017
GPS	2008 - 2011, interpolated	0.193		Stober/Wössner
GPS	2011 - 2014, average	0.186	268.03	Stober/Hönes

Tab. 6: Ice flow velocities from satellites PALSAR and Sentinel-1, compared to GPS ground measurements

Tab. 6: Eisfließgeschwindigkeiten abgeleitet von Satelliten PALSAR und Sentinel-1 im Vergleich zu GPS Bodenmessungen.

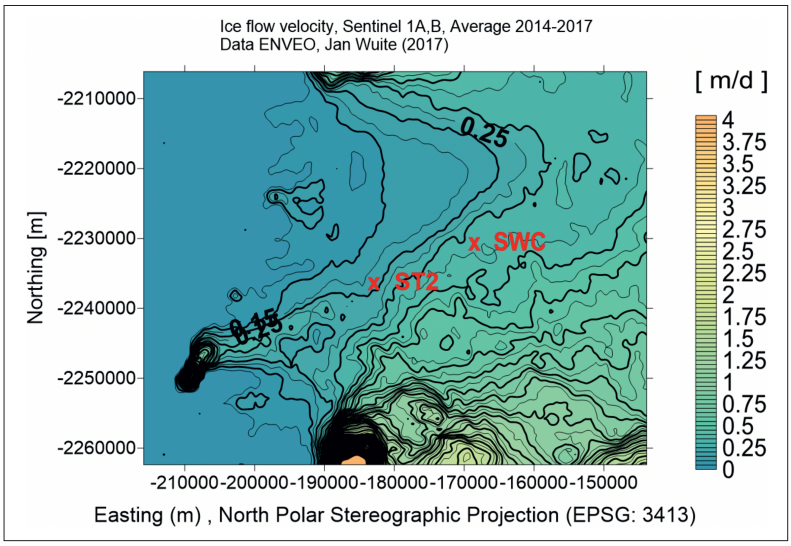

Fig. 23: Map of ice flow velocities averaged 2014–2017 around the Swiss Camp/ST2 area from Sentinel 1A+B. North Polar Stereographic Projection (EPSG: 3413). Data ENVEO/J.WUITE 2017.

Abb. 23: Karte der durchschnittlichen Eisfließgeschwindigkeiten im Zeitraum 2014-2017, im Großraum der Gebiete Swiss Camp/ST2, abgeleitet aus Sentinel 1A+B. Darstellung in North Polar Stereographic Projection (EPSG: 3413). Daten von ENVEO/J.WUITE 2017.

only Sentinel-1 and PALSAR were comparable (Table 6) with the GPS ground measurements.

The most recent remote sensing digital velocity data from Sentinel-1 is distributed by ENVEO with data averaged from October 2014 to September 2017 (WUITE 2017, personal comm.) The horizontal velocity is provided in true metres per day, towards Easting and Northing direction of a grid spacing 250 m in North Polar Stereographic Projection (EPSG: 3413). The map around SWC and ST2 with interpolated isolines of flow velocity is demonstrated in Fig. 23. The interpolated values for SWC and ST2 are included in Table 6.

At SWC, Sentinel-1 (2015) and GPS coincide well within the expected errors (GPS: ±0.002 m/d), PALSAR (2009/2010) differs significantly with slower velocity. At ST2, slower Sentinel velocities appear that agree better with PALSAR. Both PALSAR and Sentinel were measured in winter, while GPS was achieved as average from summer to summer. Seasonal variations with deceleration are therefore probable, particularly in winter.

The accuracy of Sentinel is limited by errors introduced during the matching procedure used to determine the offsets of the image, both by ionospheric disturbances and geocoding errors. In the case Sentinel-1 velocities were retrieved from a single image pair the RMSE is 0.068 m/d, and for the merged S1 ice velocity map the RMSE is 0.047 m/d (NAGLER et al. 2015), that is, much worse than GPS velocities. On average, 2014–2017 at SWC and ST2 Sentinel show an increased velocity by 10 and 5 % respectively. Considering the great local variety near the drainage catchment of the Jakobshavn Isbrae, (clearly visible in Fig. 23), the Sentinel velocities can be said to agree well with the GPS ground truth.

5. SUMMARY

The investigations of the Hochschule für Technik Stuttgart (Stuttgart University of Applied Sciences) make a unique, 23-year (1991–2014) long-term data set of ground measurements for elevation change, ice flow velocity and deformation available. Admittedly the research areas are spatially limited and they cannot be representative of all Greenland. They are, however, situated in the catchment of the Ilulissat glacier that drains 6.5 % of the entire Greenlandic ice sheet. Since 1991, the ice sheet surface elevation has decreased 14.5 m at Swiss Camp, located near the equilibrium line altitude (ELA), more than 30 km from the ice sheet margin. The rate of thinning is increasing over time. The rate of ice flow at Swiss Camp is increasing, while at the lower-situated ST2 it is decreasing. The longitudinal strain rate between both survey areas is negative, so compression exist with a positive dynamic component for the mass balance. Elevation changes are not constant over an area. There exist local variable elevation changes, which are probably due to different albedo.

In transient equilibrium, the surface mass balance and horizontal divergence of ice flux are equal, with submergent ice flow balancing net accumulation in the accumulation area, and emergent ice flow balancing net runoff in the ablation area. Ice sheet thinning occurs in two ways, either via ice dynamic thinning, due to changes in horizontal divergence of ice flux, or surface mass balance thinning, due to increased surface melting and runoff. While we document that the ice-sheet is thinning at both ST2 and Swiss Camp, both of which are situated in the contemporary ice-sheet ablation area, it is important to understand the mechanism of this thinning.

Since 1991, the ice sheet surface elevation has decreased 14.4 m (equivalent to 13 m w.e.), of which the majority appears to be due to surface mass balance, or enhanced meltwater runoff. Ice dynamics, or increasing horizontal divergence of ice flux, however, appear to be responsible for a non-trivial portion of this ice-sheet thinning (2.3 m or 18 %). The digital elevation models were used as ground truths for validation of satellite altimetry, such as CryoSat-2, ICESat, Operation IceBridge, and TerraSAR-X.

For future works the following recommendations can be given. For comparison of elevation changes with meteorological data the geodetic campaigns should be performed preferably every year. The strain rate analysis should be based on more stakes and better geometric configuration of the stake network. Than

a three-dimensional evaluation over all the area would become possible (RAWIEL 2001). For validation of satellite products the DEM should cover a larger area of at least 10 × 10 km^2. All these recommendations would substantially increase the fieldwork.

The project presented in this paper was terminated with the field campaign of 2014.
The data will be stored in the PANGAEA data base, hosted by the Alfred Wegener Institute, Helmholtz Center for Polar and Marine Research (AWI), Bremerhaven:https://www.pangaea.de/?t=Cryosphere&offset=10&f.location%5B%5D=Greenland

AUTHOR CONTRIBUTIONS

MS was the leading scientist for all campaigns, conducted fieldwork on all campaigns and was responsible for the evaluation of all data and the discussion of results. JH supported several field campaigns and evaluated the GPS-data.

ACKNOWLEDGEMENTS

The author cordially thanks to all contributors and reviewers of the research activities. The project received financial and logistical support from: (1) German Research Foundation/ Deutsche Forschungsgemeinschaft (DFG). Projects No. STO 242-1/1 and RA 1832-1/1; (2) DVW, Gesellschaft für Geodäsie, Geoinformation und Landmanagement (travel support for students); (3) Sponsors of various industrial enterprises; (4) Alfred-Wegener-Institut (AWI), Helmholtz-Zentrum für Polar- und Meeresforschung (Field Equipments, clothing); (5) ETH Zürich (Prof. Dr. A. Ohmura, Dr. H. Blatter). Field cooperation, Use of Swiss Camp 1991–1996; (6) Prof. Dr. K. Steffen, (logistics, AWS-Data), Cooperative Institute for Research in Environmental Sciences (CIRES), Boulder/USA, now: Eidgenössische Forschungsanstalt für Wald, Schnee und Landschaft (WSL), Zürich).

Data acquisition and scientific cooperation was supported by: (1) Prof. Dr. Jason Box, Geological Survey of Denmark and Greenland (GEUS), Kopenhagen; (2) Dipl.-Ing. (FH) Jörg Hepperle and Dipl.-Ing. (FH) Jürgen Kreutter, Stuttgart University of Applied Sciences; (3) Prof. Dr. Paul Rawiel and Prof. Dr. Peter Breuer, Stuttgart University of Applied Sciences; (4) Prof. Dr. Konrad Steffen (WSL Zürich/CIRES Boulder).

References

Bamber. J.L., Griggs, J.A., Hurkmans, R.T.W.L., Dowdeswell, J.A., Gogineni, S.P., Howat, I., Mouginot, J., Paden, J., Palmer, S., Rignot, E. & Steinhage D. (2013): A new bed elevation dataset for Greenland.- The Cryosphere 7: 499–510.

Banwell, A.F., Willis, I.C., Arnold, N.S., Messerli, A., Rye, C.R., Tedesco, M., & Aahlstrøm, A.P. (2012): Calibration and evaluation of a high-resolution surface mass-balance model for Paakitsoq, West Greenland.- Journal of Glaciology 58 (212): 1047-1062

Bartholomew, I., Nienow, P., Sole, A., Mair, D., Cowton, T. & King, M.A. (2012): Short-term variability in Greenland Ice Sheet motion forced by time-varying meltwater drainage: Implications for the relationship between subglacial drainage system behaviour and ice velocity.- J. Geophys. Res. 117: F03002, doi:10.1029/2011JF002220.

Bondzio, J.H, Seroussi, H., Morlighem, M., Kleiner, T., Rückamp, M., Humbert, A. & Larour, E.Y. (2016): Modelling calving front dynamics using a level-set method: Aapplication to Jakobshavn Isbræ, West Greenland.- The Cryosphere 10: 497–510, doi:10.5194/tc-10-497-2016.

Bondzio, J.H., Morlighem, M., Seroussi, H., Kleiner, T., Rückamp, M., Mouginot, J., Moon, T., Larour, E.Y. & Humbert, A. (2017): The mechanisms behind Jakobshavn Isbræ's acceleration and mass loss: A 3-D thermomechanical model study.- Geophys. Res. Lett. 44: 6252–6260, doi:10.1002/2017GL073309.

Box, J. & Steffen, K. (2000): Greenland Climate Network (GC-NET), Data Reference, Version: November 10, 2000, Program for Arctic Regional Climate Assessment (PARCA).- Cooperative Institute for Research in Environmental Sciences (CIRES), University of Colorado, Boulder, USA.

Box, J.E., Fettweis, X., Stroeve, J.C., Tedesco, M., Hall, D.K. & Steffen, K. (2012): Greenland ice sheet albedo feedback: thermodynamics and atmospheric drivers.- The Cryosphere 6: 821-839.

Braithwaite, R.J. (1985): Calculation of degree-days for glacier-climate research.- Zeitschrift für Gletscherkunde und Glazialgeologie 20: 1-8.

Braithwaite, R.J. (1995): Positive degree-day factors for ablation on the Greenland ice sheet studies by energy-balance modelling.- J. Glaciol.: 41: 153-160.

Businger, J.A. & Fleagle, R.G. (1980): An Introduction to Atmospheric Physics, International Geophysics Series Vol. 25 (2nd ed.). Academic Press, San Diego, 1-432.

Catania, G., Neumann, T. & Price, S. (2008): Characterizing englacial drainage in the ablation zone of the Greenland ice sheet.- Journal of Glaciology: 54(187): 567-578.

Colgan, W., Steffen, K., Scott M.C., Lamb, W., Abdalati, W., Rajaram, H., Motyka, R., Phillips, T. & Anderson, R. (2011a): An increase in crevasse extent, West Greenland: Hydrologic implications.- Geophysical Research Letters: 38: L18502, doi:10.1029/2011GL048491.

Colgan, W., Rajarham, H., Anderson, R., Steffen, K., Phillips, T., Joughin, I., Oughin, H, Zwally, J. & Abdalati, W. (2011b): The annual glaciohydrology cycle in the ablation zone of the Greenland ice sheet: Part 1, Hydrology model.- Journal of Glaciology: 57 (204): 697-709.

Colgan, W.T. (2011): Investigating the influence of surface meltwater on the ice dynamics of the Greenland ice sheet.- Unpublished PhD-thesis, Department of Geography, University of Colorado, http://www.william-colgan.net/pubs/ColganPhDThesis.pdf, 1-136.

Colgan, W.H., Rajaram, R., Anderson, S., Steffen, K., Zwally, J., Phillips, T. & Abdalati, W. (2012): The annual glaciohydrology cycle in the ablation zone of the Greenland Ice Sheet: Part 2, Observed and Modeled Ice Flow.- Journal of Glaciology 58 (207): 51-64.

Colgan, W., Abdalati, W., Citterio, M., Csatho, B., Fettweis, X., Luthcke, S., Moholdt, G., Simonsen, S.B. & Stober, M. (2015): Hybrid glacier Inventory, Gravimetry and Altimetry (HIGA) mass balance product for Greenland and the Canadian Arctic.- Remote Sensing of Environment 168: 24–39.

Doyle, S.H., Hubbard, A., van de Wal, R.S.W., Box, J.E., van As, D.K. Scharrer, K., T.W. Meierbachtol, T.W.,. Smeets, P.C. J.P., Harper, J.T., Johansson, E., Mottram, R.H., Mikkelsen, A.B., Wilhelms, F., Patton, H., Christoffersen, P. & Hubbard, B. (2015): Amplified melt and flow of the Greenland ice sheet driven by late-summer cyclonic rainfall.- Nature Geoscience, 8: 647-653, doi:10.1038/ngeo2482.

DTU (2005): Digital height data (Underground, surface, ice thickness).- DTU Space, Microwaves and Remote Sensing, Denmarks Technical University, Kopenhagen, (personal communication).

ESA (2003): CryoSat Science Report / European Space Agency, Version: March 2003, http://www,cryosat,de/cryosat/.

ESA (2007): CryoSat Mission and Data Description / European Space Agency, Version: January 2007, Document Nr,: CS-RP-ESA-SY-0059, http://www,cryosat,de/cryosat/.

Fausto, R.S., Box, J.E., Vandecrux, B., van As, D., Steffen, K., MacFerrin, M., Machguth, H., Colgan, W., Koenig, L., McGrath, D., Charalampidis, Ch. & Braithwaite, R. (2018): A Snow Density Dataset for Improving Surface BoundaryConditions in Greenland Ice Sheet Firn Modeling.- Frontiers in Earth Science 6 (51), doi:10.3389/feart.2018.00051.

Giese, M., Kaczkowski, J., Lange, A., Stiegert, C., Wiegratz, J., Zakrzewski, P. & Wanninger, L. (2011): Berechnungsdienste für Precise Point Positioning (PPP).- Allgemeine Vermessungs-Nachrichten 3: 89-94.

Glen, J.W. (1958): The flow law of ice: A discussion of the assumptions made in glacier theory, their experimental foundations and consequences,- IASH Publ. 47: 171–183.

Helm, V., Humber, A. & Miller, H. (2014): Elevation and elevation change of Greenland and Antarctica derived from CryoSat-2.- The Cryosphere 8: 1539–1559, doi:10.5194/tc-8-1539-2014.

Hönes, M. (2015): Auswertung der Grönlandkampagne 2014 und zusammenfassender Vergleich der Höhenänderung, Fließgeschwindigkeit und klimatischer Faktoren 1991 bis 2014.- Unpubl. Bachelor Thesis, HFT Stuttgart.

Hock, R. (2005): Glacier melt: A review of processes and their modelling.- Progress in Physical Geography 29: 362-391.

Hoffman, M.J., Catania, G.A., Neumann, T.A., Andrews, L.C. & Rumrill, J.A. (2011): Links between acceleration, melting, and supraglacial lake drainage of the western Greenland Ice Sheet.- J. Geophys. Res. 116: F04035, doi:10,1029/2010JF001934.

Homann, C., Möller, D., Salbach, H. & Stengele, R. (1996): Die Weiterführung der geodätischen Arbeiten der Internationalen Glaziologischen Grönland-Expedition (EGIG) durch das Institut für Vermessungskunde der TU Braunschweig 1987-1993.- Deutsche Geodätische Kommission bei der Bayerischen Akademie der Wissenschaften, Reihe B, Angewandte Geodäsie, Heft 303: 59-70.

Hooke, R. (1998): Principles of Glacier Mechanics.- Prentice Hall, New Jersey, 1-428.

IGS (2009): IGS products, International GNSS Service, http://igscb.jpl.nasa.gov/components/prods.html.

Jezek, K.C. (2012): Surface elevation and velocity changes on the south-central Greenland ice sheet: 1980–2011.- Journal of Glaciology: 58(212), doi:10.3189/2012JoG12J031.

Joughin, I., Smith, B.E. & Howat, I. (2018): A complete map of Greenland ice velocity derived from satellite data collected over 20 years.- Journal of Glaciology 64(243): 1-11.

Kettemann, R. (2011): Precise Point Positioning: A GNSS Method for Georeferencing Isolated Regions.- Applied Geoinformatics for Society and Environment (AGSE), 36-40, Nairobi, Kenya.

Konzelmann, T. & Braithwaite, R.J. (1995): Variations of ablation, albedo and energy balance at the margin of the Greenland ice sheet, Kronprins Christian Land, eastern north Greenland.- Journal of Glaciology 41: 174–82.

Kouba, J. & Héroux, P. (2000): GPS Precise Point Positioning using IGS orbit Products.- GPS Solutions 5(2), 12-28, doi:10.1007/PL00012883.

Korth, W., Adler, W., Hofmann, U., Münster, U., Polte, F. & Rückamp, M. (2008): Bestimmung von Eishöhenänderungen in Grönland.- Zeitschrift für Geodäsie, Geoinformation und Landmanagement - zfv 133 (6): 135-148.

Korth, W. & Hofmann, U. (2010): Eishöhenänderungen im südlichen Grönland.- Forum GeoBau, Band 1, Beuth Hochschule Berlin, 29-38.

Korth, W, & Hofmann, U. (2010): Grönlandexpedition 2010, erste Ergebnisse.- Terra Nostra 2010/1, Tagungsbeiträge der 24. Internationalen Polartagung der Deutschen Gesellschaft für Polarforschung, Obergurgl 2010.

Korth, W. & Hofmann, U. (2012): Eismassenänderungen im südlichen Grönland zwischen 1912 und 2012.- Internationale Geodätische Woche, Obergurgl 2012.

Krieger, G., Zink, M., Bachmann, M., Bräutigam, B., Schulze, D., Martone, M., Rizzoli, P., Steinbrecher, U., Antony, J.W., de Zan, F., Hajnsek, I., Papathanassiou, K., Kugler, F., Cassola, M.R., Younis, M., Baumgartner, S., López-Dekker, P., Prats, P. & Moreira, A. (2013): TanDEM-X: A radar interferometer with two formation-flying satellites.- Acta Astronautica 89: 83-98.

Li, J. & Zwally, J. (2011): Modeling of firn compaction for estimating ice-sheet mass change from observed ice-sheet elevation change.- Annals of Glaciology 52 (59): 1-7.

Lüthi, M., Vieli, A., Moreau, L., Joughin, I., Reisser, M., Small, D. & Stober, M. (2016): A Century of geometry and velocity evolution at Eqip Sermia, West Greenland.- Journal of Glaciology 62 (234): 640-654, doi:10.1017/jog,2016.38.

Machguth, H; Thomsen, H.H., Weidick, A., Ahlstrøm, A.P., Abermann, J., Andersen, M.L., Andersen, S.B., Bjørk, A.A., Box, J.E., Braithwaite, R.J., Bøggild, C.E., Citterio, M., Clement, P., Colgan, W., Fausto, R.S., Gleie, K., Gubler, S., Hasholt, B., Hynek, B., Knudsen, N.T., Larsen, S.H., Mernild, S.H., Oerlemans, J., Oerter, H., Olesen, O.B., Smeets, C. J. P., Steffen, K, Stober, M., Sugiyama, S., van As, D., van den Broeke, M.R. & van de Wal, R.S.W. (2016): Greenland surface mass-balance observations from the ice-sheet ablation area and local glaciers.- Journal of Glaciology, 62 (235): 861-887. doi:10.1017/jog.2016.75.

Mcgrath, D., Colgan,W., Steffen, K., Lauffenburger, P. & Balog, J. (2011): Assessing the summer water budget of a moulin basin in the Sermeq Avannarleq ablation region, Greenland ice sheet.- Journal of Glaciology 57/205: 954-964.

Mernild, S. H., Mote, T. L. & Liston, G.L. (2011): Greenland ice sheet melt extent and trends: 1960-2010.- Journal of Glaciology, 57(204): 621-628.

Mireault, Y., Tétreault, P., Lahaye, F., Héroux, P. & Kouba, J. (2008): Online Precise Point Positioning.- GPS World, September 2008: 59-64.

Morriss, B.F., Hawley, R.L, Chipman, J.W., Andrews, L.C., Catania, G.A., Hoffman, M.J., M. P. Lüthi, M.P. & Neumann, T.A. (2013): A ten-year record of supraglacial lake evolution and rapid drainage in West Greenland using an automated processing algorithm for multispectral imagery.- The Cryosphere Discuss. 7: 3543–3565.

Nagler, T., Rott, H., Hetzenecker, M., Wuite, J. & Potin, P. (2015): The sentinel-1 mission: new opportunities for ice sheet observations.- Remote Sens. 7: 9371-9389, doi:10.3390/rs70709371.

National Snow & Ice Data Center (NSDIC): http://nsidc,org/data/icesat/faq,html#alt7, Altimetry Products, FAQ Nr. 7.

Natural Resources Canada (NRCan), Canadian Spatial Reference System CSRS, www.geod.nrcan.gc.ca.

Nghiem, S.V., Hall, D.K., Mote, T.L., Tedesco, M., Albert, M.R., Keegan, K., Shuman, C.A., Di Girolamo, N.E. & Neumann, G. (2012): The extreme melt across the Greenland ice sheet in 2012.- Geophysical Research Letters, 39: L20502, doi:10.1029/2012GL053611.

Ohmura, A., Steffen, K., Blatter, H., Greuell, W., Rotach, M., Konzelmann, T., Laternser, M., Ouchi, A. & Steiger, D. (1991): ETH Greenland Expedition, Progress Report No. 1, Department of Geography, Swiss Federal Institute of Technology Zurich.

Paterson, W.S.B. (1994): The Physics of Glaciers (third edition).- Pergamon, Oxford, 1-480.

Price, S.F., Payne, A.J., Catania, G.A. & Neumann, T.A. (2008): Seasonal acceleration of inland ice via longitudinal coupling to marginal ice.- Journal of Glaciology 54(185): 213-219.

Rawiel, P. (2001): Dreidimensionale kinematische Modelle zur Analyse von Deformationen an Hängen, Deutsche Geodätische Kommission (DGK), München, Reihe C, Nr. 533.

Rizzoli, P., Brautigam, B., Kraus, T., Martone, M. & Krieger, G. (2012): Relative height error analysis of Tandem-X.- ISPRS Journal of Photogrammetry and Remote Sensing 73: 30-38.

Rizos, C., Janssen, V., Roberts, G. & Grinter, T. (2012): Precise Point Positioning: Is the Era of Differential GNSS Positioning Drawing to an End?, FIG Working Week 2012, Rome, Italy, 6-10 May 2012.

Ryan, J.C., Hubbard, A., Box, J.E., Brough, S., Cameron, K.M. Cook, J.M., Cooper, M., Doyle, S.H., Edwards, A., Holt, T., Irvine-Fynn, T., Jones, Ch., Pitcher, L.H., Rennermalm, A.K., Smith, L.C., Stibal, M. & Snooke, N. (2017): Derivation of High Spatial Resolution Albedo from UAV Digital Imagery: Application over the Greenland Ice Sheet.- Frontiers in Earth Science, May 2017, doi:10.3389/feart.2017.00040.

Ryan, J.C., Hubbard, A., Stibal, M., Irvine-Fynn, T.D., Cook, J., Smith, L.C., Cameron,K. & Box, J. (2018): Dark zone of the Greenland Ice Sheet controlled by distributed biologically-active impurities.- Nature Communications 9: 1-10, doi:10.1038/s41467-018-03353-2

Price, S.F., Payne, A.J., Catania, G.A. & Neumann, T.A. (2008): Seasonal acceleration of inland ice via longitudinal coupling to marginal ice.- J. Glaciol. 54: 213-219.

Rumrill, J.A. (2009): Analysis of spatial and temporal variations in strain rates near Swiss Camp, Greenland.- Unpublished Master Thesis, University of Vermont.

Scott, M. (2014): Reflectivity of Greenland Ice Sheet in late summer hit new low in 2014, Map and graph from NOAA Climate Gov. and Fiona Martin, based on data from J.E. Box, Geological Survey of Denmark and Greenland.

Sirguey, P., Still, H., Cullen, N., Dumont, M., Arnaud, Y. & Conway, J. (2016): Reconstructing the mass balance of Brewster Glacier, New Zealand, using MODIS-derived glacier-wide albedo.- The Cryosphere 10: 2465–2484.

Schenk, T., Csatho, B., van der Veen, C. & McCornick, D. (2014): Fusion of multi-sensor surface elevation data for improved characterization of rapidly changing outlet glaciers in Greenland.- Remote Sensing of Environment 149: 239-251.

Steffen, K., Huff, R. & Rial, J. (2006): Greenland – Accumulation and Melt Layers: Regional Climatology, Process Studies, and Seismicity, University of Colorado at Boulder, Cooperative Institute for Research in Environmental Sciences (CIRES), Progress Report to NASA, December 2006.

Steffen, K., Colgan, L., Bayou, N. & Philips, T. (2011): Surface processes of the Greenland ice sheet under a warming climate, Progress Report to National Aeronautics and Space Administration, Cryospheric Program and National Science Foundation, June 2011.

Steffen, K., Colgan, W., Bayou, N. with contributions by Stober, M., Rawiel, P., Hepperle, J. & Wössner, R. (2012): Surface processes, Glacio-Hydrology, and Englacial modeling of the Greenland Ice Sheet, University of Colorado at Boulder (CIRES), NASA Progress Report, April 2012.

Stober, M. (1995): Untersuchungen zum Refraktionseinfluß bei der trigonometrischen Höhenmessung auf dem grönländischen Inlandeis.- Festschrift Draheim/Kuntz/Mälzer, Geod. Inst. Univ. Karlsruhe, 259-272.

Stober, M. (2001): Zur Berechnung der Höhenänderung des grönländischen Inlandeises aus geodätisch bestimmten Strainraten.- Forschungsbericht 2001 der HfT Stuttgart, Veröffentlichungen der HfT Stuttgart, Band 55: 51-55.

Stober, M. & Hepperle, J. (2006): Changes in Ice Elevation and Ice Flow-Velocity in the Swiss Camp Area (West Greenland) between 1991 and 2006.- Polarforschung 76(3): 109-118.

Stober, M. (2008): Relations between horizontal strain and ice elevation change. The Dynamics and Mass Budget of Arctic Glaciers. Workshop, 29-31 January 2008, Obergurgl, Institute for Marine and Atmospheric Research Utrecht, Utrecht University, Extended Abstracts, 113-116.

Stober, M., Rawiel, P., Hepperle, J. & Wössner, R. (2013a): Long-term observations (1991–2011) of elevation change and ice flow velocity in the swiss-Camp area (West Greenland), The Dynamics and Mass Budget of

Arctic Glaciers, IASC Network of Arctic Glaciology, 9-12 January 2012, GEUS Rapport No. 3, 68-72.

Stober, M., Hepperle, J. & Wössner, R. (2013b): Precise Point Positioning (PPP) and its application to studies in ice dynamics in West Greenland, IASC Workshop & Network on Arctic Glaciology annual meeting, 26-28 February 2013. Obergurgl (Austria), Editor C.H. Tijm-Reijmer, ISBN: 978-90-393-6003-3.

Stober, M. (2016): Langzeitbeobachtung zur Massenbilanz und Dynamik im Bereich des Swiss Camp, West Grönland, Presentation at: Arbeitskreis Polargeodäsie und Glaziologie der Deutschen Gesellschaft für Polarforschung, Dresden, 7.-8.4.2016.

Tedesco, M., Box, J.E., Capellen, J., Fettweis, X., Mote, T., Van De Wal, R.S.W., Smeets, C. & Wahr. J. (2014): Arctic Report Card, Update for 2014, The Greenland Ice Sheet.

Trenberth, K.E. & Fasullo, J.T. (2013): An apparent hiatus in global warming?- Earth's Future 1: 19-32, doi:10.1002/2013EF000165.

Van de Wal, R.S.W., Oerlemanns, J. & Hage, J.C. (1992): A study of ablation variations on the tongue of Hintereisferner, Austrian Alps.- Journal of Glaciology 38: 319–24.

Weber, M. (2005): Mikrometeorologische Prozesse bei der Ablation eines Alpengletschers.- Unpublished PhD Thesis, Institut für Meteorologie und Geophysik der Universität Innsbruck, 1-258.

Weidick, A. & Bennike, O. (2007): Quarternary glaciation history and glaciology of Jakobshavn Isbrae and the Disko Bugt region, West Greenland: a review.- Bulletin of the Glaciological Survey of Denmark and Greenland 14: 1-78.

Welsch, W. (1982): Description of homogenous horizontal strains and some remarks to their analysis, Deutsche Geodätische Kommission, Reihe B, 258: 188-205.

Zumberge, J.F., Heftin, M. B., Jefferson, D.C. Watkins, M. M. & Webb, F.H. (1997): Precise point positioning for the efficient and robust analysis of GPS data from large networks.- Journal of Geophysical Research, 102 (B3): 5005-5017.

Zwally, H.J., Abdalati, W., Herring, T., Larsen, K., Saba, J. & Steffen, K. (2002): Surface melt-induced acceleration of Greenland ice-sheet flow.- Science 297: 218-222.